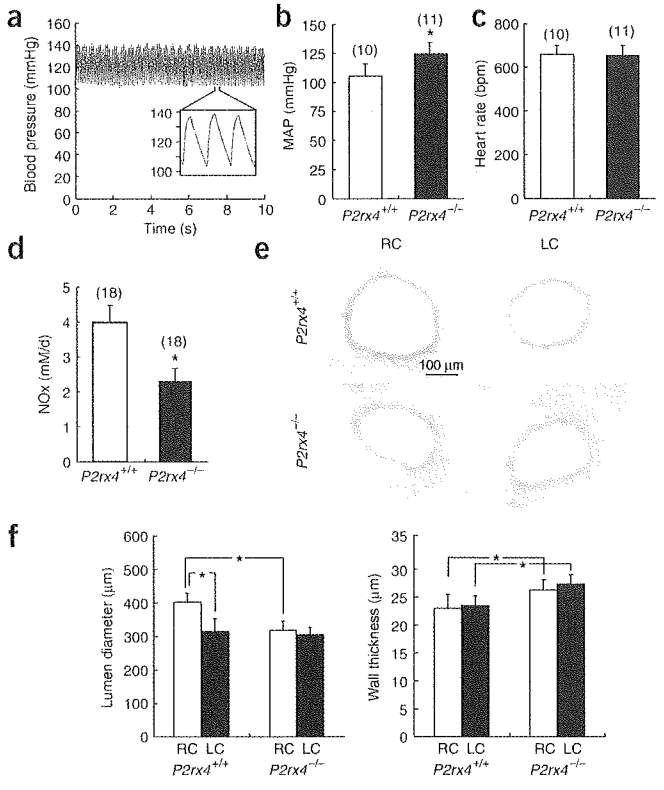

Figure 4 *P2rx4*$^{-/-}$ mice show higher blood pressure with less production of NO and impaired blood flow–induced vascular remodeling. (**a**) Representative pressure recordings of unrestrained, conscious *P2rx4*$^{-/-}$ mice 1 week after implantation of a radiotelemeter in the thoracic aorta through the left carotid artery. (**b**) Mean arterial pressure (MAP). Values are 24-h averages of the basal MAP obtained 1 week after surgery. MAP was significantly higher in *P2rx4*$^{-/-}$ mice than in wild-type mice. (**c**) Heart rate. No difference in heart rate was seen between the two types of mice. (**d**) The amount of nitrite and nitrate (NOx) in 24-h urine samples was significantly lower in *P2rx4*$^{-/-}$ mice than in wild-type mice. Sample numbers are indicated in parentheses. $^*P < 0.01$. (**e**) Hematoxylin-eosin–stained cross-sections of the right common carotid artery (RC) and left common carotid aretery (LC). In wild-type mice, the diameter of the lumen of the LC became smaller than that of the RC. By contrast, the diameter of the LC in *P2rx4*$^{-/-}$ mice did not change. Medial thickening was observed in the arteries of *P2rx4*$^{-/-}$ mice. (**f**) Quantitative analysis of changes in lumen diameter and wall thickness. After ligation the diameter of the LC decreased significantly in wild-type mice, but not in *P2rx4*$^{-/-}$ mice. The diameter of the RC of *P2rx4*$^{-/-}$ mice was significantly smaller than that of wild-type mice. The wall thickness of the RC and LC of *P2rx4*$^{-/-}$ mice was significantly greater than that of wild-type mice. Data are expressed as the mean ± s.d. $^*P < 0.01$. $n = 10$ and 12 mice for wild-type and *P2rx4*$^{-/-}$ mice, respectively.

including ion channels, tyrosine receptors, caveolae, G proteins, adhesion molecules and cytoskeletons, have been considered as potential candidates for shear stress receptors[21]. Multiple signaling pathways are activated through these receptors downstream of shear stress sensing[5]. For instance, the phosphorylation of protein kinases, such as extracellular signal–regulated kinase (ERK1/2), p130 Crk-associated substrate (Cas) and focal adhesion kinase (FAK), occurs in endothelial cells immediately after exposure to shear stress[22,23]. Flow-induced phosphorylation of ERK1/2, but not of Cas or FAK, was partially inhibited in *P2rx4*$^{-/-}$ mice (**Supplementary Fig. 4** online). Thus, P2X4-mediated signaling events do not seem to be independent, but instead are involved in cross-talk with other signaling pathways.

The gene-knockout approach has contributed to the clarification of the physiological and pathological roles of each P2X receptor subtype. For instance, mice lacking P2X1 show reduced contraction of vas deferens and male infertility[24]. Studies of *P2rx3*$^{-/-}$ mice have indicated that P2X3 is crucial for peripheral pain responses and the afferent pathway that controls urinary bladder volume reflexes[25,26]. Pharmacological blockade of P2X4 receptors has shown them to be involved in the tactile allodynia that occurs after nerve injury[27]. Here we show that P2X4 channels have a crucial role in controlling vascular tone and vascular remodeling. But the abovementioned roles may not hold in all other vascular beds, as the expression of P2X4 varies greatly among different vascular beds[12]. Deficiency of P2X4 severe enough to abolish ATP- or flow-induced Ca^{2+} influx probably reduces endothelial production of NO, which in turn increases vascular tone. In addition to its role as a vasodilator, NO negatively regulates proliferation of smooth muscle[28]; thus, a reduction in NO production may cause an increase in vascular wall thickness. These changes in vascular tone and vessel wall geometry may explain why *P2rx4*$^{-/-}$ mice are hypertensive. Vascular smooth muscle predominantly expresses P2X1; thus, it is unlikely that deficiency of P2X4 directly affects the tone of vascular smooth muscle. But the possibility remains that deficiency of P2X4 may impair nervous system function and increase vascular tone. Although further studies are needed to resolve this issue, our results provide insight that will allow better understanding of the molecular mechanisms involved in the regulation of vascular tone and vascular remodeling through ATP and its receptors. This in turn may lead to the development of new therapies for the control of blood pressure disorders.

METHODS

Northern blot analysis. We evaluated *P2rx4* mRNA levels using northern blot analysis, as previously described[10].

Competitive PCR. We performed competitive PCR as previously described[10].

Cell culture. We performed primary culture of microvessel endothelial cells from murine lung tissue as previously reported[29].

Immunohistochemistry. We performed detection of the P2X4 receptor and von Willebrand factor (NeoMarkers) using antibodies as previously described[10].

Determination of $[Ca^{2+}]_i$. We placed the coverslip on which we loaded endothelial cells with Indo-1/AM (Dojindo) in a parallel plate–type flow chamber (FCS2, Bioptechs, Inc.), and perfused Hanks balanced salt solution (HBSS) through the chamber with a peristaltic pump to stimulate cells at 37 °C. We monitored flow-induced changes in $[Ca^{2+}]_i$ with a confocal laser scanning system (MRC-1000UV, Bio-Rad) equipped with an ultraviolet argon ion laser, as previously described[10,13].

Measurement of NO production. We measured the concentration of nitrite and nitrate (NOx) in urine by fluorometric assay with a spectrofluorometer. We evaluated production of NO in cells by real-time imaging of NO with a fluorescent indicator, diaminofluorescein-2 diacetate (DAF-2 DA; 10 μM, Daiichi Pure Chemicals) as previously described[17].

Gene transfer by adenovirus vectors. We constructed adenovirus vectors containing murine *P2rx4* cDNA or cDNA encoding green fluorescent protein (GFP) using the Adeno-X Expression System (BD Biosciences) according to the manufacturer's protocol. We infected cultured endothelial cells with 50 plaque-forming units/cell of either adenovirus vector.

Mice. All protocols were approved by the Institutional Animal Care and Use Committee of the University of Tokyo.

Measurement of blood pressure. We measured blood pressure in unrestrained, conscious mice using a commercially available telemetry and computer-based data acquisition system (Data Sciences International) according to a previously described method[30]. Briefly, we anesthetized mice with halothane inhalation. We then implanted a pressure-sensing catheter in the thoracic aorta through the left carotid artery, and we placed a radio-telemetry transmitter under the skin along the right flank. After recovery from the anesthesia, we returned the mice to their home cages (placed atop telemetry receivers), where we continuously monitored their blood pressure and heart rate.

Diameter measurements in arterioles and arteries. We anesthetized mice with urethane, and we cannulated a jugular vein to facilitate the injection of chemicals. We observed microcirculation in the cremaster muscle with an intravital microscope. One of the branches of an arteriole was compressed with a glass micropipette (Occluder) to stop blood flow, and the other branch, in which the blood flow increased, was examined for changes in diameter. We filmed the microcirculation with a CCD camera, and analyzed changes in the diameter of large arterioles having a baseline diameter of 40-80 μm using images shown on a television monitor.

Mesenteric resistance-artery preparation. We isolated mesenteric artery segments that had an internal diameter of ~200 μm, cannulated them at both ends and mounted them in a video-monitored perfusion system. We bathed segments in an organ bath containing Krebs solution and perfused them at flow rates ranging from 0 to 150 μl/min at a constant pressure (60 mmHg). We monitored the pressure in both ends of the artery segment with pressure transducers.

External carotid artery ligation. We ligated the left external carotid artery of mice at its origin with 11-0 nylon sutures. After 2 weeks, we anesthetized mice with urethane and perfused them through the left ventricle with PBS at a constant pressure (100 mmHg), and then perfusion-fixed them with freshly depolymerized 4% paraformaldehyde in PBS. We excised and post-fixed both common carotid arteries overnight at 4 °C. We excised parallel segments of the left and right common carotid arteries at the midpoint of the vessels, and after embedding them in O.C.T. (Tissue-Tek), we cut cross-sections (3–5 μm thick) for hematoxylin-eosin staining and Elastica Masson staining. We morphometrically analyzed the carotid arteries by video microscopy. The image was displayed on a computer monitor, and the vessel perimeter was measured using the US National Institutes of Health image software. The perimeter of the vessel lumen was taken as the circumference of a circle (C) and lumen diameter (D) was determined from the equation $D = C/\pi$, assuming that the vessel cross-sections were circular *in vivo*. We measured medial wall thickness on images of Elastica Masson–stained vessels as the linear distance from the inner elastic lamina to the external elastic lamina at a magnification of ×200. We measured four sites 90° apart in each of two serial vessel sections, and we averaged the values.

Statistical analysis. We evaluated statistical significance by an ANOVA and a Bonferonni adjustment was applied to the results of a *t* test with SPSS software (SPSS Inc). Data are expressed as means ± s.d. $P < 0.01$ was regarded as statistically significant.

Note: Supplementary information is available on the Nature Medicine website.

ACKNOWLEDGMENTS

This study was partly supported by Grants-in-Aid for Scientific Research from the Japan Society for the Promotion of Science and by a grant from the Japan Health Sciences Foundation. The authors are grateful to U. Chung and F. Kugimiya (Divisions of Tissue Engineering and Sensory & Motor System Medicine, Faculty of Medicine, University of Tokyo) for suggestions on technical issues in establishing of adenovirus vectors. We also thank Y. Sawada for technical assistance.

COMPETING INTERESTS STATEMENT

The authors declare that they have no competing financial interests.

Published online at http://www.nature.com/naturemedicine/
Reprints and permissions information is available online at http://npg.nature.com/reprintsandpermissions/

1. Kamiya, A. & Togawa, T. Adaptive regulation of wall shear stress to flow change in the canine carotid artery. *Am. J. Physiol.* **239**, H14–H21 (1980).
2. Guyton, J.R. & Hartley, C.J. Flow restriction of one carotid artery in juvenile rats inhibits growth of arterial diameter. *Am. J. Physiol.* **248**, H540–H546 (1985).
3. Hudlicka, O., Brown, M. & Egginton, S. Angiogenesis in skeletal and cardiac muscle. *Physiol. Rev.* **72**, 369–417 (1992).
4. Langille, B.L. & O'Donnell, F. Reductions in arterial diameter produced by chronic decreases in blood flow are endothelium-dependent. *Science* **231**, 405–407 (1986).
5. Davies, P.F. Flow-mediated endothelial mechanotransduction. *Physiol. Rev.* **75**, 519–560 (1995).
6. Burnstock, G. Release of vasoactive substances from endothelial cells by shear stress and purinergic mechanosensory transduction. *J. Anat.* **194**, 335–342 (1999).
7. North, R.A. Molecular physiology of P2X receptors. *Physiol. Rev.* **82**, 1013–1067 (2002).
8. Vial, C., Roberts, J.A. & Evans, R.J. Molecular properties of ATP-gated P2X receptor ion channels. *Trends Pharmacol. Sci.* **25**, 487–493 (2004).
9. Burnstock, G. & Knight, G.E. Cellular distribution and functions of P2 receptor subtypes in different systems. *Int. Rev. Cytol.* **240**, 31–304 (2004).
10. Yamamoto, K. *et al.* P2X(4) receptors mediate ATP-induced calcium influx in human vascular endothelial cells. *Am. J. Physiol. Heart Circ. Physiol.* **279**, H285–H292 (2000).
11. Glass, R. & Burnstock, G. Immunohistochemical identification of cells expressing ATP-gated cation channels (P2X receptors) in the adult rat thyroid. *J. Anat.* **198**, 569–579 (2001).
12. Ray, F.R., Huang, W., Slater, M. & Barden, J.A. Purinergic receptor distribution in endothelial cells in blood vessels: a basis for selection of coronary artery grafts. *Atherosclerosis* **162**, 55–61 (2002).
13. Yamamoto, K., Korenaga, R., Kamiya, A. & Ando, J. Fluid shear stress activates Ca^{2+} influx into human endothelial cells via P2X4 purinoceptors. *Circ. Res.* **87**, 385–391 (2000).
14. Mo, M., Eskin, S.G. & Schilling, W.P. Flow-induced changes in Ca^{2+} signaling of vascular endothelial cells: effect of shear stress and ATP. *Am. J. Physiol.* **260**, H1698–H1707 (1991).
15. Milner, P., Bodin, P., Loesch, A. & Burnstock, G. Rapid release of endothelin and ATP from isolated aortic endothelial cells exposed to increased flow. *Biochem. Biophys. Res. Commun.* **170**, 649–656 (1990).
16. Fleming, I., Bauersachs, J. & Busse, R. Calcium-dependent and calcium-independent activation of the endothelial NO synthase. *J. Vasc. Res.* **34**, 165–174 (1997).
17. Kojima, H. *et al.* Detection and imaging of nitric oxide with novel fluorescent indicators: diaminofluoresceins. *Anal. Chem.* **70**, 2446–2453 (1998).
18. Koller, A., Sun, D., Huang, A. & Kaley, G. Corelease of nitric oxide and prostaglandins mediates flow-dependent dilation of rat gracilis muscle arterioles. *Am. J. Physiol.* **267**, H326–H332 (1994).
19. Masuda, H. *et al.* Increase in endothelial cell density before artery enlargement in flow-loaded canine carotid artery. *Arteriosclerosis* **9**, 812–823 (1989).
20. Rudic, R.D. *et al.* Direct evidence for the importance of endothelium-derived nitric oxide in vascular remodeling. *J. Clin. Invest.* **101**, 731–736 (1998).
21. Resnick, N. *et al.* Fluid shear stress and the vascular endothelium: for better and for worse. *Prog. Biophys. Mol. Biol.* **81**, 177–199 (2003).
22. Okuda, M. *et al.* Shear stress stimulation of p130(cas) tyrosine phosphorylation requires calcium-dependent c-Src activation. *J. Biol. Chem.* **274**, 26803–26809 (1999).
23. Li, S. *et al.* Fluid shear stress activation of focal adhesion kinase. Linking to mitogen-activated protein kinases. *J. Biol. Chem.* **272**, 30455–30462 (1997).
24. Mulryan, K. *et al.* Reduced vas deferens contraction and male infertility in mice lacking P2X1 receptors. *Nature* **403**, 86–89 (2000).
25. Cockayne, D.A. *et al.* Urinary bladder hyporeflexia and reduced pain-related behaviour in *P2X3*-deficient mice. *Nature* **407**, 1011–1015 (2000).
26. Vlaskovska, M. *et al. P2X3* knock-out mice reveal a major sensory role for urothelially released ATP. *J. Neurosci.* **21**, 5670–5677 (2001).
27. Tsuda, M. *et al.* P2X4 receptors induced in spinal microglia gate tactile allodynia after nerve injury. *Nature* **424**, 778–783 (2003).
28. Garg, U.C. & Hassid, A. Nitric oxide-generating vasodilators and 8-bromo-cyclic guanosine monophosphate inhibit mitogenesis and proliferation of cultured rat vascular smooth muscle cells. *J. Clin. Invest.* **83**, 1774–1777 (1989).
29. Kuhlencordt, P.J. *et al.* Role of endothelial nitric oxide synthase in endothelial activation: insights from eNOS knockout endothelial cells. *Am. J. Physiol. Cell Physiol.* **286**, C1195–C1202 (2004).
30. Butz, G.M. & Davisson, R.L. Long-term telemetric measurement of cardiovascular parameters in awake mice: a physiological genomics tool. *Physiol. Genomics* **5**, 89–97 (2001).

The EMBO Journal (2005) 24, 3881–3894 | © 2005 European Molecular Biology Organization | All Rights Reserved 0261-4189/05
www.embojournal.org

THE EMBO JOURNAL

Ligand-induced transrepression by VDR through association of WSTF with acetylated histones

Ryoji Fujiki[1], Mi-sun Kim[1], Yasumasa Sasaki[1], Kimihiro Yoshimura[1], Hirochika Kitagawa[1] and Shigeaki Kato[1,2,*]

[1]The Institute of Molecular and Cellular Biosciences, The University of Tokyo, Bunkyo-ku, Tokyo, Japan and [2]ERATO, Japan Science and Technology, Kawaguchi, Saitama, Japan

We have previously shown that the novel ATP-dependent chromatin-remodeling complex WINAC is required for the ligand-bound vitamin D receptor (VDR)-mediated transrepression of the 25(OH)D_3 1α-hydroxylase (1α(OH)ase) gene. However, the molecular basis for VDR promoter association, which does not involve its binding to specific DNA sequences, remains unclear. To address this issue, we investigated the function of WSTF in terms of the association between WINAC and chromatin for ligand-induced transrepression by VDR. Results of *in vitro* experiments using chromatin templates showed that the association of unliganded VDR with the promoter required physical interactions between WSTF and both VDR and acetylated histones prior to VDR association with chromatin. The acetylated histone-interacting region of WSTF was mapped to the bromodomain, and a WSTF mutant lacking the bromodomain served as a dominant-negative mutant in terms of ligand-induced transrepression of the 1α(OH)ase gene. Thus, our findings indicate that WINAC associates with chromatin through a physical interaction between the WSTF bromodomain and acetylated his tones, which appears to be indispensable for VDR/promoter association for ligand-induced transrepression of 1α(OH)ase gene expression.

The EMBO Journal (2005) **24,** 3881–3894. doi:10.1038/sj.emboj.7600853; Published online 27 October 2005
Subject Categories: chromatin & transcription
Keywords: acetylated histone; transrepression; VDIR; VDR; WSTF

Introduction

Lipophilic ligands, such as fat-soluble vitamins A and D, as well as thyroid/steroid hormones, are thought to exert their physiological effects through transcriptional control of target genes via cognate nuclear receptors (NRs) (Mangelsdorf *et al*, 1995). NRs form a gene superfamily, and they act as ligand-inducible activators. A number of coregulator complexes that support ligand-dependent transcription control have been identified, and these complexes can be classified into three categories according to function (Glass and Rosenfeld, 2000). The first coregulator complex class regulates transcriptional control directly, through a physical interaction with general transcription factors and RNA polymerase II (Rachez *et al*, 1998; Gu *et al*, 1999). Members of the second coregulator complex class modify histone tails covalently, for example by acetylation, in promoter nucleosomal arrays (Onate *et al*, 1995; Kamei *et al*, 1996; Heinzel *et al*, 1997; Yanagisawa *et al*, 2002). The major function of the last class of complexes is chromatin remodeling, which involves the ATP-dependent dynamic remodeling of chromatin structure (Ito *et al*, 1997; Fyodorov and Kadonaga, 2001; Lemon *et al*, 2001; Narlikar *et al*, 2002; Kitagawa *et al*, 2003). Chromatin-remodeling complexes utilize energy from ATP hydrolysis to rearrange nucleosomal arrays in a non-covalent manner. As chromosomal DNA is generally packed as nucleosomal arrays, chromatin-remodeling complexes are thought to render specific promoter regions accessible to other coregulator complex classes and sequence-specific regulators.

Recently, we identified a novel, multifunctional, ATP-dependent chromatin-remodeling complex, designated WINAC, which consists of 13 subunits (Kitagawa *et al*, 2003). It contains SWI/SNF chromatin-remodeling complex components and DNA replication-related factors. Vitamin D receptor (VDR) interacts with WINAC in a ligand-independent manner through the Williams syndrome transcription factor (WSTF). WSTF belongs to bromodomain adjacent to a zinc-finger motif (BAZ) protein family. Members of this family harbor both a PHD finger and a bromodomain in their C-terminal domain (Jones *et al*, 2000). As bromodomains have been recently shown to bind acetylated histones, it is possible that WSTF serves as an adaptor protein for acetylated histones, facilitating the association between WINAC and chromatin (Dhalluin *et al*, 1999; Winston and Allis, 1999; Jacobson *et al*, 2000; Hassan *et al*, 2002).

Expression of the 25(OH)D_3 1α-hydroxylase (1α(OH)ase) gene, a key enzyme in vitamin D biosynthesis, is negatively regulated by vitamin D (Takeyama *et al*, 1997; Yoshizawa *et al*, 1997; Murayama *et al*, 1998). We recently reported that a bHLH-type activator, VDR-interacting repressor (VDIR), directly binds to the negative vitamin D response element (1αnVDRE) in the human 1α(OH)ase gene promoter, thus activating transcription (Murayama *et al*, 2004). However, ligand-induced association between VDR and VDIR results in ligand-induced transrepression of 1α(OH)ase gene expression. This occurs through the switching of coregulator complexes from histone acetyltransferase (HAT) coactivator complexes to histone deacetylase (HDAC) corepressors upon VDIR binding to 1αnVDRE (Murayama *et al*, 2004). However, the molecular basis of VDR targeting to 1αnVDRE in the chromatinized 1α(OH)ase gene promoter remained unclear.

In the present study, we demonstrate, using chromatin templates *in vitro*, that both ligand-free VDR and WINAC avidly associate with the 1α(OH)ase gene promoter when the promoter region is reconstituted as a nucleosomal array. The

*Corresponding author. The Institute of Molecular and Cellular Biosciences, The University of Tokyo, 1-1-1 Yayoi, Bunkyo-ku, Tokyo 113-0032, Japan. Tel.: +81 3 5841 8478; Fax: +81 3 5841 8477; E-mail: uskato@mail.ecc.u-tokyo.ac.jp

Received: 23 May 2005; accepted: 6 October 2005; published online: 27 October 2005

WSTF bromodomain in WINAC appears to serve as a chromatin-targeting module that escorts ligand-free VDR to the promoter via a physical interaction with acetylated histones. Thus, our findings show that WINAC associates with chromatin through a physical interaction between the WSTF bromodomain and acetylated histones. This apparently contributes to the association between unliganded VDR and the promoter, resulting in a ligand-induced transrepression of human 1α(OH)ase gene expression.

Results

Involvement of WSTF in ligand-induced transrepression by VDR/VDIR of the 1α(OH)ase gene promoter

It has previously been shown that VDIR activates transcription via specific binding to 1αnVDRE in the promoter (Murayama *et al*, 2004). The association of liganded VDR with VDIR then inhibits VDIR transactivation function through recruitment of an HDAC corepressor complex, resulting in ligand-induced transrepression (Murayama *et al*, 2004). Although WSTF was previously shown to be involved in 1α(OH)ase gene regulation (Kitagawa *et al*, 2003; Kato *et al*, 2004), the function of WSTF, with respect to ligand-induced VDR/VDIR transrepression, remained unclear.

We employed a transient expression assay using MCF7 cells, which express the 1α(OH)ase gene endogenously, and a luciferase reporter gene plasmid containing two consensus 1αnVDRE sequences recognized by VDIR. These sequences confer negative responsiveness to 1α,25$(OH)_2D_3$ in gene repression. 1α,25$(OH)_2D_3$ transrepressed transcription of the reporter gene, and this repression was enhanced in the presence of VDR/RXR expression (Figure 1A).

We further assessed whether endogenous VDR, VDIR and WSTF were responsible for ligand-induced negative responsiveness of the 1α(OH)ase gene, using RNAi in a transient expression assay, in which a reporter gene was driven by the native promoter. The analysis confirmed that RNAi down-regulated expression of the target endogenous factors without modulating the expression levels of the other factors (Figure 1B). We confirmed that WSTF-RNAi and VDIR-RNAi are able to abrogate the transrepression function of VDIR and WSTF, respectively, and VDR-RNAi eliminates both of them (Figure 1C). These results show that it is likely that WSTF mediates the ligand-induced transrepression of the 1α(OH)ase gene, together with VDR and VDIR.

WSTF associates with VDIR in a ligand-dependent manner

Based on our findings that WSTF appears to play a role in ligand-induced VDR/VDIR transrepression, we further examined the complex formed by these three factors in MCF-7 cells using an immunoprecipitation assay. As unliganded VDR was reported to associate with NCoR corepressor complex (Glass and Rosenfeld, 2000), the corepressor dissociation of exogenous VDR was observed in response to ligand binding (Figure 2A, lanes 3 and 4). As previously reported (Kitagawa *et al*, 2003; Kato *et al*, 2004; Murayama *et al*, 2004), while VDR associated with WSTF irrespective of 1α,25$(OH)_2D_3$ binding, 1α,25$(OH)_2D_3$ binding enhanced the interaction between VDR and VDIR (Figure 2A, lanes 3–8). Exogenous WSTF co-immunoprecipitated with exogenous VDIR in a ligand-dependent manner, and with endogenous NCoR corepressor complex components (NCoR, mSin3 and HDAC2) in the presence of 1α,25$(OH)_2D_3$ (Figure 2A, lanes 7 and 8). Furthermore, we found that an HDAC inhibitor trichostatin A (TSA)-released HDAC activity was contained in immunoprecipitates of exogenous FLAG-WSTF, and this activity was enhanced in a ligand-dependent manner (Figure 2B). The ligand-dependent association of VDR/WSTF with VDIR was also observed for endogenous proteins in MCF7 cells (Figure 2C). This ligand binding is presumably required for the association between VDR/WSTF and VDIR, and it results in recruitment of an HDAC corepressor complex.

We tested this hypothesis using an *in vitro* GST pull-down assay on a series of bacterially expressed GST-fused WSTF mutants (Figure 2D). The WSTF m1 domain (aa 163–576, illustrated as a shaded box above the panel) was found to interact with *in vitro*-translated VDR, irrespective of 1α,25$(OH)_2D_3$ binding (Figure 2E, upper panel). No clear association of VDR with the other regions was detected, even in the presence of 1α,25$(OH)_2D_3$. We then assessed the interaction of VDIR with the WSTF mutants. While none of the WSTF regions exhibited physical interaction with VDIR, in the presence of 1α,25$(OH)_2D_3$-bound VDR, an association between WSTF and VDIR was detected (Figure 2E, middle and lower panels). Together, these findings suggest that while WSTF interacts with VDR, VDIR is stably recruited only when VDR is liganded.

WSTF mediates 1α(OH)ase gene promoter occupancy of ligand-unbound VDR

To test whether WSTF was recruited to VDIR via liganded VDR in the nuclei of living cells, we performed a chromatin immunoprecipitation (ChIP) assay using endogenous proteins and the native 1α(OH)ase gene promoter. In agreement with previous reports (Kitagawa *et al*, 2003; Murayama *et al*, 2004), VDIR was constitutively bound to 1αnVDRE, while the NCoR corepressor complex components were recruited to the promoter 45 min after the addition of 1α,25$(OH)_2D_3$

Figure 1 WSTF enhances 1α,25$(OH)_2D_3$-induced transrepression of 1α(OH)ase gene expression, but not transactivation by VDIR. (**A**) Coordinate transrepression of the 1α(OH)ase gene by VDR, WSTF and VDIR in a luciferase reporter assay. MCF7 cells were transfected with a luciferase reporter gene expression vector containing 1αnVDRE (×2) driven by a TATA promoter (0.4 μg), pML-CMV (2 ng), and either pSG5-rat VDR and pSG5-rat RXRα (0.2 μg each), pcDNA3-VDIR (0.1 μg), pcDNA3-WSTF (0.1[+], 0.3[++] μg), or combinations thereof in the presence or absence of 1α,25$(OH)_2D_3$ (10^{-8} M) (Kitagawa *et al*, 2003; Murayama *et al*, 2004). Bars in each graph show the fold change in luciferase activity relative to basal activity obtained in the absence of ligand. All values are means±s.d. for at least three independent experiments. (**B**) Gene-specific knockdown of WSTF, VDIR or VDR by RNAi was confirmed by Western blots using anti-WSTF, -VDIR, -VDR and β-actin (as a control). Whole-cell extracts were prepared from MCF7 cells transfected with 0.3 μg of double-stranded siRNA and further cultured for 48 h. (**C**) Effect of gene-specific knockdown of endogenous factors, WSTF, VDIR and VDR on 1α(OH)ase gene expression in a luciferase reporter assay. MCF7 cells were transfected with 0.3 μg of the indicated siRNAs, 48 h after the transfection luciferase reporter gene containing 1α(OH)ase native promoter was transfected again into the cells. Luciferase activity was assessed after 12 h culture in the presence or absence of 1α,25$(OH)_2D_3$ (10^{-8} M).

(Figure 3A). SNF2h, an ISWI chromatin-remodeling complex ATPase, was used as a negative control. As WSTF RNAi remarkably attenuated the promoter occupancy of VDR in the absence of ligand, WSTF appeared to facilitate the binding of ligand-unbound VDR to the 1αnVDRE region (Figure 3A). The occupancy of VDR and WSTF was undetectable in the 1α(OH)ase-distal region, confirming promoter-specific binding of the factors. A Re-ChIP assay was performed to

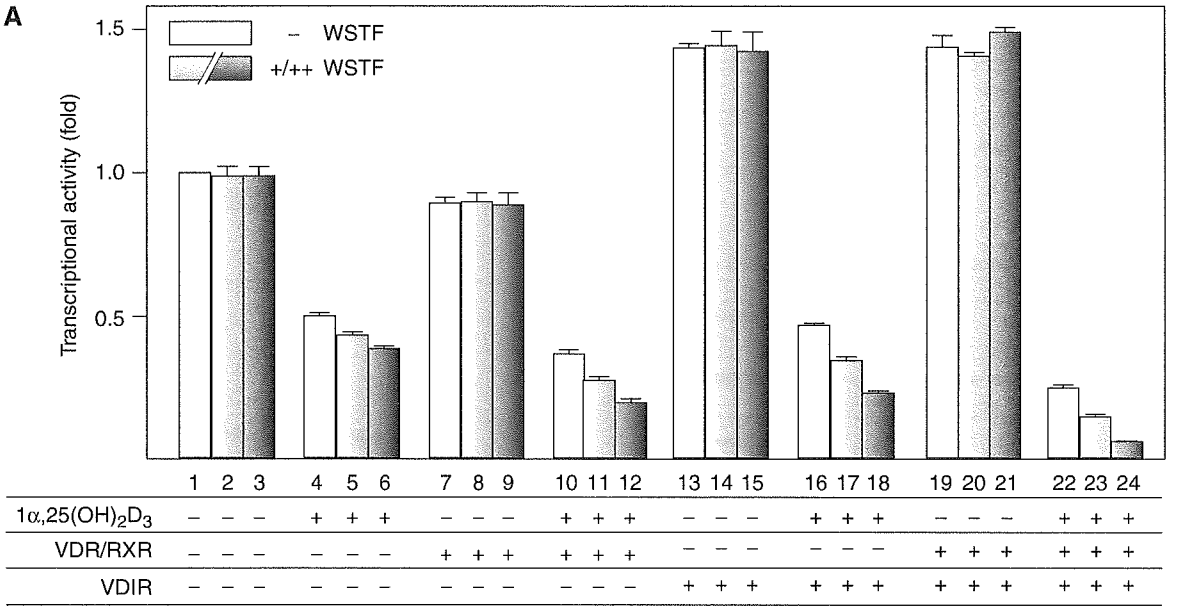

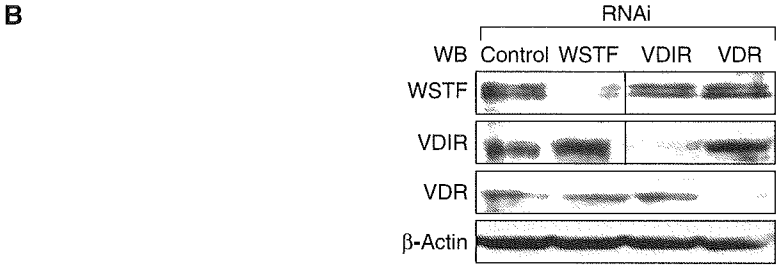

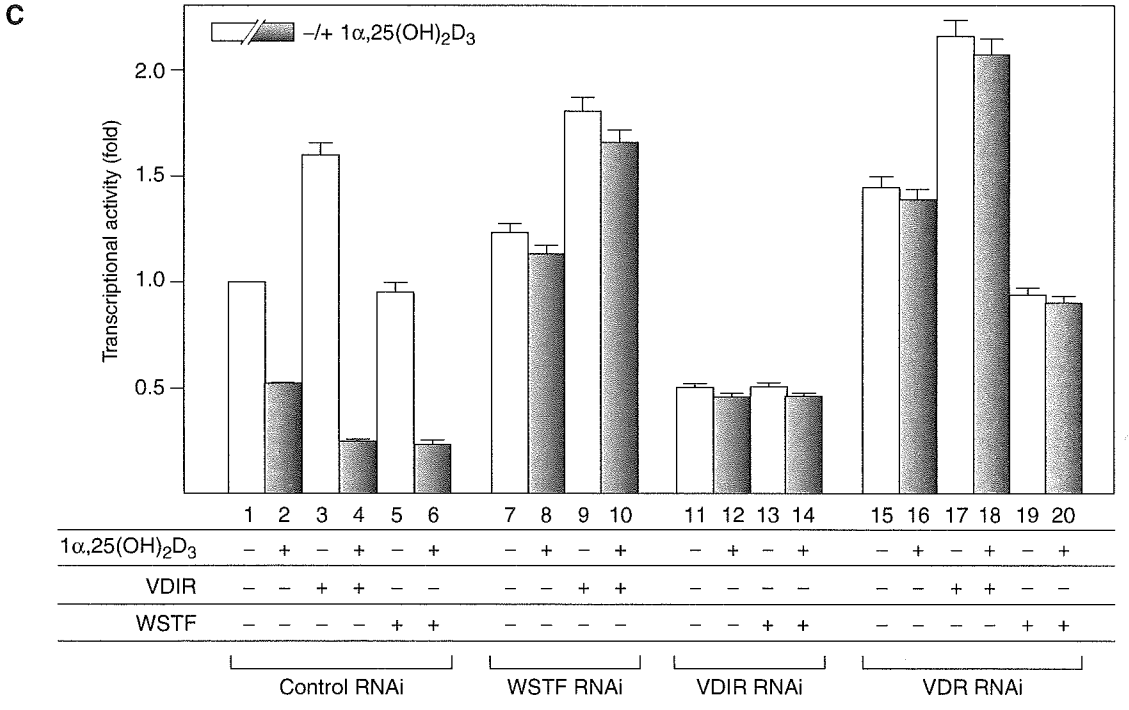

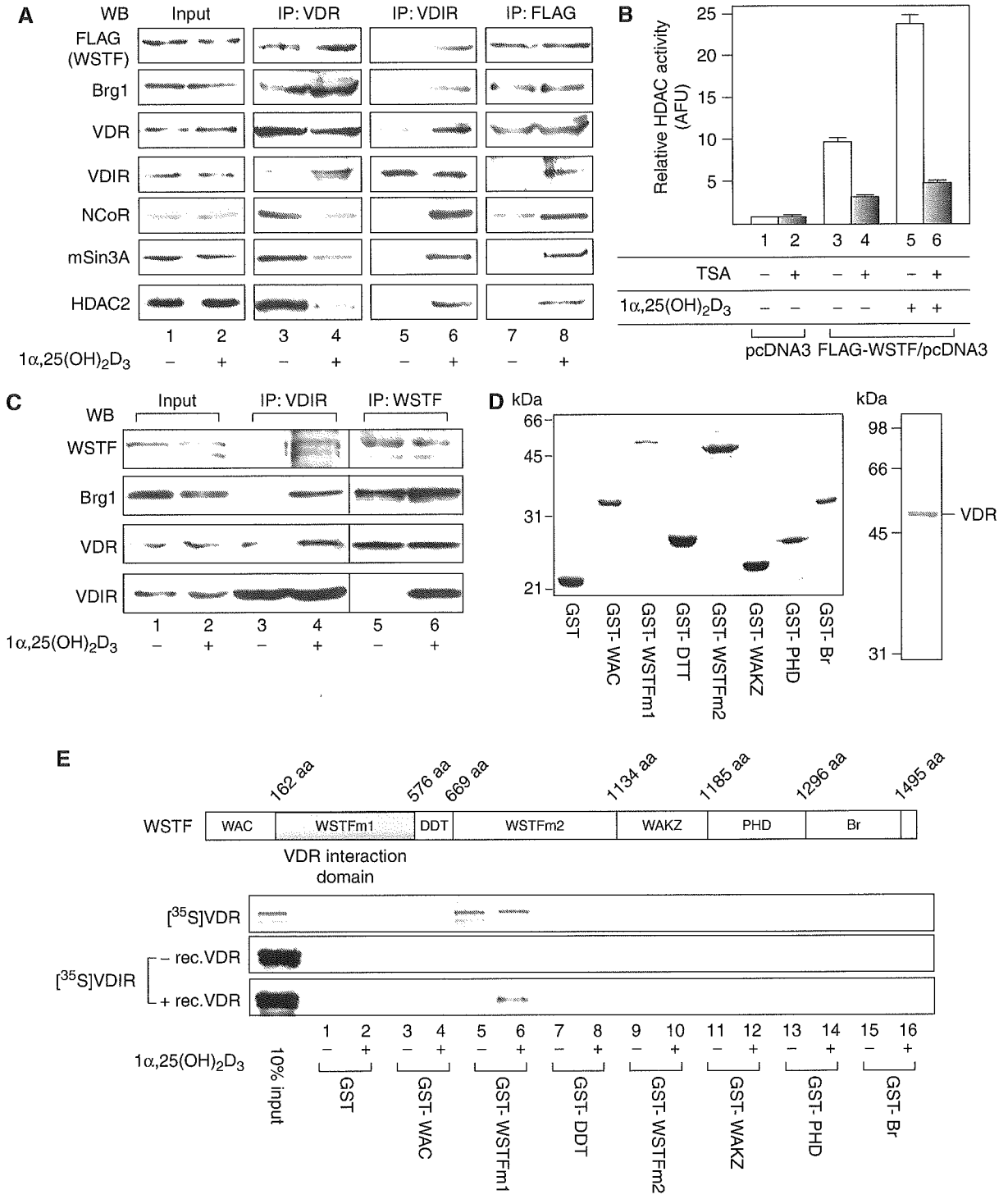

Figure 2 WSTF interacts with VDIR through 1α,25(OH)2D3-bound VDR. (**A**) Exogenous WSTF interacted with exogenous VDIR and endogenous corepressors in an $1\alpha,25(OH)_2D_3$-dependent manner *in vivo*. MCF7 cells were transfected with 0.3 μg of WSTF, VDR and VDIR expression vector. The panels show results of immunoprecipitation with anti-VDR, -VDIR or -FLAG (WSTF) antibodies, followed by Western blot analysis using the indicated antibodies. (**B**) WSTF associates with HDAC activity in a ligand-dependent manner. MCF7 cells were transfected with pcDNA3 or FLAG-WSTF/pcDNA3 and the extracted cell lysates were then immunoprecipitated with anti-FLAG M2 resin. HDAC activity in the immunoprecipitates was measured by fluorometric detection using an HDAC assay kit. (**C**) $1\alpha,25(OH)_2D_3$-dependent interaction between endogenous WSTF and VDIR *in vivo*. MCF7 cells cultured with or without $1\alpha,25(OH)_2D_3$ for 12 h were subjected to immunoprecipitation with anti-WSTF or anti-VDIR antibodies. Immunoprecipitates were Western blotted with specific antibodies as shown on the left. (**D**) SDS–PAGE gels of a series of GST-fused WSTF deletion mutants (left panel) and recombinant VDR (right panel) were visualized by CBB staining. Recombinant proteins were expressed in *Escherichia coli* and purified by affinity chromatography. (**E**) GST pull-down assay. Schematic diagrams of the WSTF deletion mutants used are illustrated. ^{35}S-labeled VDR translated *in vitro* was incubated with deletion mutants immobilized onto glutathione-Sepharose beads in the presence or absence of $1\alpha,25(OH)_2D_3$ (10^{-6} M). Bound proteins were resolved by SDS–PAGE followed by autoradiography (upper panel). Autoradiographs show ^{35}S-labeled VDIR, preincubated with (lower panel) or without (middle panel) cold recombinant VDR, bound to the GST-fused mutants immobilized on beads (Murayama *et al*, 2004).

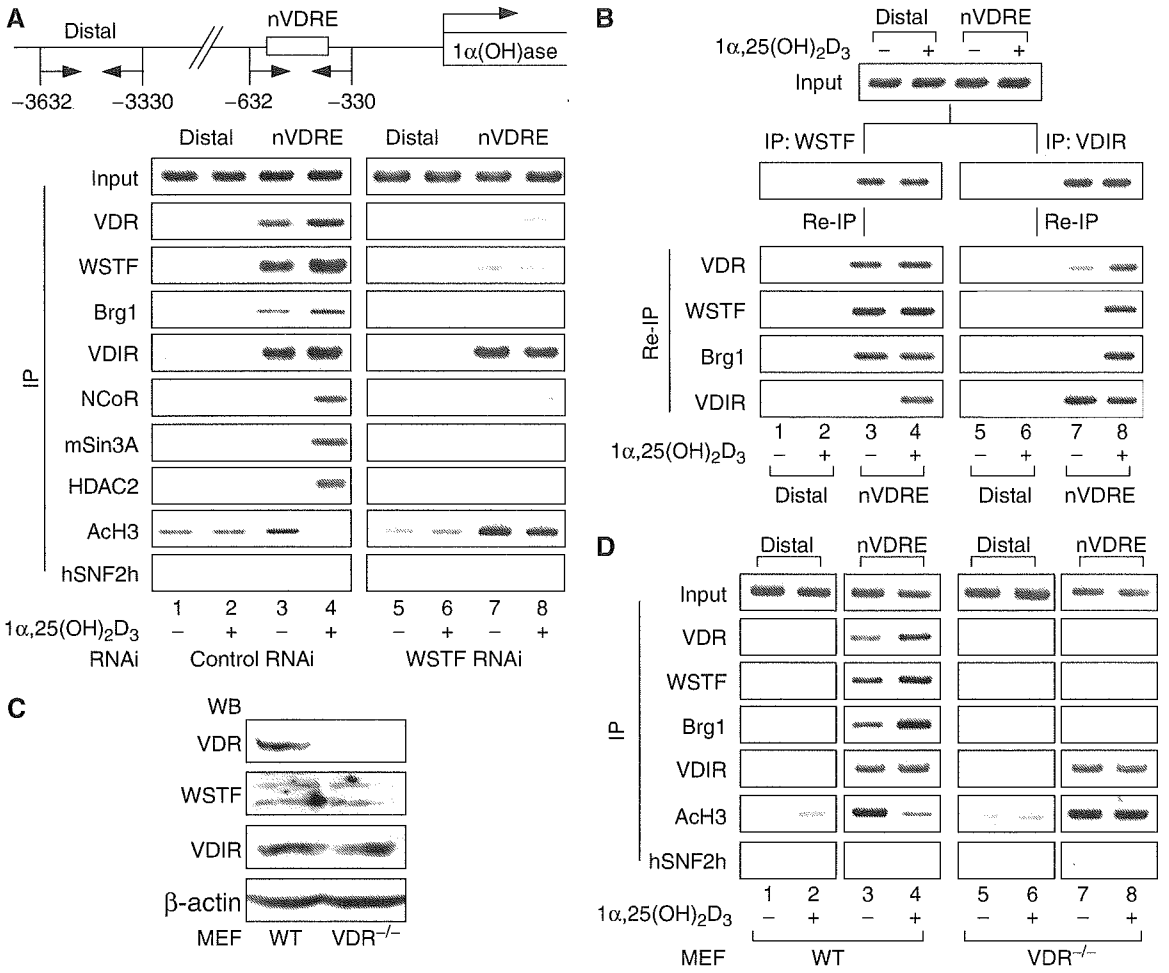

Figure 3 VDR is indispensable for ligand-induced promoter assembly of the WINAC and HDAC corepressor complex. (**A**) Recruitment of VDR, WSTF, VDIR and other coregulators to the 1α(OH)ase gene promoter *in vivo*, as shown by ChIP analysis. Soluble chromatin was prepared from MCF7 cells treated with 1α,25(OH)$_2$D$_3$ (10^{-8} M) for 45 min and immunoprecipitated with the indicated antibodies. Extracted DNA samples were amplified using primer pairs that covered the 1α(OH)ase negative VDRE region (1αnVDRE) (Kitagawa *et al*, 2003; Murayama *et al*, 2004) or a distal region (3 kb upstream of 1αnVDRE) as a control. (**B**) Recruitment of ligand-free VDR/WSTF complexes to the 1α(OH)ase gene promoter, shown by the re-chromatin immunoprecipitation (Re-ChIP) assay. Chromatin prepared from MCF7 cells cultured in the presence or absence of 1α,25(OH)$_2$D$_3$ (10^{-8} M) for 45 min was subjected to the ChIP procedure with the indicated antibodies and immunoprecipitated using the antibodies as shown on the left. (**C**) Cessation of VDR expression in VDR$^{-/-}$ MEF cells was confirmed by Western blot analysis. VDR$^{-/-}$ and wild-type (WT) MEF cells were generated from VDR$^{-/-}$ knockout mouse embryos and WT littermates (E 13.5). (**D**) Effect of VDR disruption in recruitment of WSTF and VDIR to the 1α(OH)ase gene promoter *in vivo* by ChIP analysis. Soluble chromatin was prepared from VDR$^{-/-}$ and WT MEF cells treated with 1α,25(OH)$_2$D$_3$ (10^{-8} M) for 45 min and subjected to the ChIP procedure as described in panel A.

verify the formation of the unliganded VDR, WSTF and VDIR complex at 1αnVDRE. Ligand-independent association of VDR and WSTF was observed in the 1αnVDRE region, while clear association of VDR with VDIR required ligand binding (Figure 3B). Finally, to verify a physiological role for VDR in WINAC promoter targeting, isolated primary mouse embryonic fibroblasts (MEFs) derived from VDR knockout mice were used, after confirming the ablation of VDR protein without changes in the expression level of VDIR and WSTF by Western blotting analysis (Figure 3C). In a ChIP assay using VDR$^{-/-}$ MEFs, VDR appeared to mediate the recruitment of these factors to the 1αnVDRE-proximal region (Figure 3D). Based on these findings, it appeared that WSTF requires VDR to target the promoter nucleosomes, and WSTF facilitates the subsequent retention of unliganded VDR. Furthermore, 1α,25(OH)$_2$D$_3$ binding appears to induce association of VDR with VDIR together with an HDAC complex to trigger ligand-induced transrepression.

Promoter targeting of unliganded VDR via WSTF requires chromatin structures

To clarify the mechanism by which WSTF targets unliganded VDR to the promoter *in vitro*, we addressed which factors are indispensable for the promoter targeting of unliganded VDR by employing an immobilized DNA/chromatin template recruitment assay. DNA fragments containing either 1αnVDRE (−60 to −615) or the 1α(OH)ase distal region (−3632 to −3032) were end-biotinylated to allow their immobilization onto streptavidin beads. These fragments were reconstituted as highly regular nucleosome arrays using recombinant dNAP1 protein and dACF complexes, along with purified histone octamers from HeLa cells and bacterially expressed histone octamers as unmodified histones for negative control (Figure 4A), as previously reported (Nakagawa *et al*, 2001; Kitagawa *et al*, 2003). The expected functions of the chromatin reconstitution factors were verified by supercoiling or standard micrococcal nuclease (MNase) digestion assays

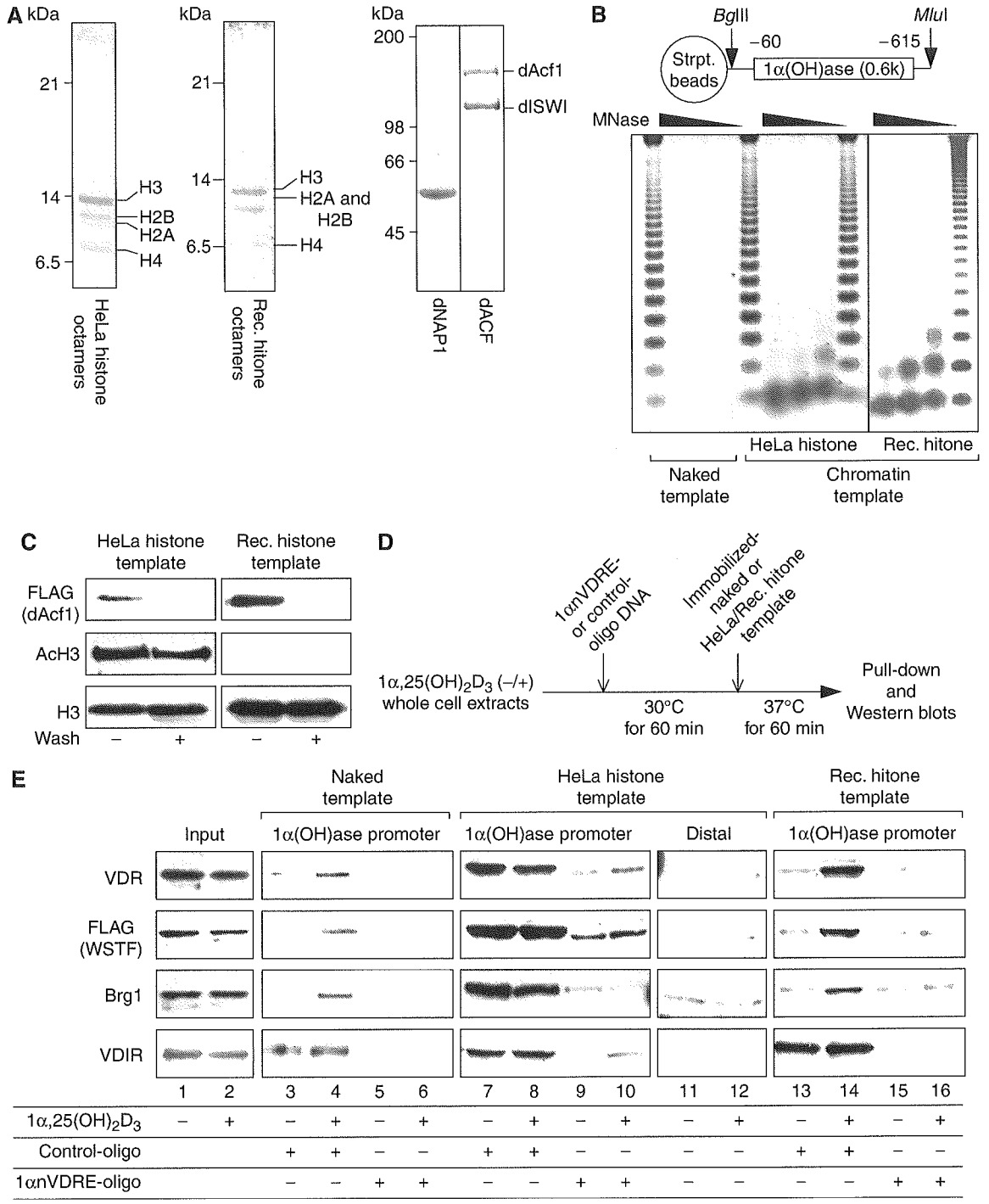

Figure 4 Chromatin structures are required to target unliganded VDR to the 1α(OH)ase promoter. (**A**) SDS–PAGE analysis of purified HeLa histone octamers, recombinant histone octamers, recombinant *Drosophila* NAP1 (dNAP1) and *Drosophila* ACF (dACF) complexes. HeLa histone octamers were purified from HeLa nuclear pellets by traditional hydroxylapatite chromatography, as described in Materials and methods. Each component of the recombinant histone octamer, H2A, H2B, H3 and H4, was expressed in an insoluble form in *E. coli* and extracted with guanidine hydrochloride. Extracted crude proteins were further purified by traditional gel filtration and ion exchange chromatography, as described previously (Luger *et al*, 1999). Affinity-tagged recombinant dNAP1 and dACF complex components (FLAG-dAcf1 and dISWI) were expressed in Sf9 cells by infection with recombinant baculoviruses and purified by affinity chromatography as described in Materials and methods. (**B**) Chromatin template containing the 1α(OH)ase gene promoter immobilized to streptavidin beads. Schematic representation of the DNA template containing the 1α(OH)ase gene promoter is illustrated above. Chromatinized template reconstituted *in vitro* was confirmed using the standard MNase digestion assay. The 123 bp ladder DNA was used as a size marker. (**C**) Immobilized template was subjected to Western blot analysis with an anti-FLAG antibody. To eliminate possible contamination by recombinant dACF complexes, immunoblotting of the beads using anti-FLAG, acetylated histone H3 and unmodified histone H3 (as a control) antibodies was performed after extensive washing with high-salt buffer. (**D**) Schematic diagram of the *in vitro*-immobilized DNA/chromatin template assay. (**E**) Stabilization of the ligand-free VDR/WSTF complex on the 1α(OH)ase promoter required chromatin structure *in vitro*. Whole-cell extracts from MCF7 cells stably expressing FLAG-WSTF treated with or without 1α,25(OH)$_2$D$_3$ (10^{-8} M) were mixed with immobilized templates. The template beads were then concentrated using a magnet and analyzed by Western blotting using the indicated antibodies.

(data not shown). Using these factors, the end-biotinylated DNA fragments were correctly reconstituted into nucleosome arrays according to the MNase digestion assay (Figure 4B). As dAcf-1 in the dACF complex is highly homologous to WSTF, chromatin templates were analyzed by Western blots to confirm the absence of dAcf-1 after final washing (Figure 4C).

Whole-cell extracts from MCF-7 cells that stably expressed FLAG-tagged WSTF treated with or without $1\alpha,25(OH)_2D_3$ were incubated with either naked or chromatin DNA templates containing 1αnVDRE. Proteins bound to the DNA templates were then analyzed by immunoblotting (Figure 4D). WSTF and VDR bound to naked DNA templates only in the presence of ligand, while VDIR stably associated with naked DNA templates even in the absence of ligand (Figure 4E, lanes 3 and 4). The specific recruitment of WSTF, together with VDR and VDIR, to 1αnVDRE was confirmed by the finding that addition of excessive synthetic 1αnVDRE oligonucleotides blocked recruitment (Figure 4E, lanes 5 and 6). In contrast, for the chromatin templates with HeLa histone octamers, recruitment of WSTF and VDR was ligand-independent (Figure 4E, lanes 7 and 8). However, WSTF and VDR were removed to significant extents from chromatinized templates by the addition of excess 1αnVDRE oligonucleotides (Figure 4E, lanes 9 and 10), indicating a role for DNA-bound VDIR in the stable association of VDR/WSTF with chromatin. This significant association of WSTF and VDR with chromatin template was not seen when the distal 1α(OH)ase gene promoter region was used (Figure 4E, lanes 11 and 12), or when the promoter region with the octamers of the unmodified histones was used (Figure 4E, lanes 13–16). This supported the significance of WSTF function in unliganded VDR recruitment to the native 1α(OH)ase promoter.

WSTF associates with acetylated nucleosomes and facilitates transcriptional repression through its C-terminal region, which contains the bromodomain

As a member of the BAZ protein family, WSTF harbors two characteristic domains, designated the bromodomain and the PHD finger, in its C-terminal region. Because these domains are present in a number of chromatin-remodeling factors (Ito *et al*, 1997; Dhalluin *et al*, 1999; Winston and Allis, 1999; Jacobson *et al*, 2000; Hassan *et al*, 2002), we speculated that the WSTF bromodomain and the PHD finger play a role in the observed association between WSTF and chromatin. To address whether these domains served as the direct contact site for histone octamers, we performed *in vitro* histone binding experiments with purified histone octamers from HeLa cells, and GST fusion proteins containing the bromodomain and PHD finger regions. We also prepared anti-FLAG immunoprecipitates having HDAC activity from whole lysates of MCF7 cells with $1\alpha,25(OH)_2D_3$ (Figure 2B), in order to deacetylate the HeLa histone octamers (Figure 5A). The results indicated that the WSTF bromodomain bound to the histone octamers only when histones were preincubated with the anti-FLAG immunoprecipitates and TSA, while the PHD finger bound the octamers only weakly (Figure 5B, even number lanes). Because bromodomains are generally known to serve as a motif responsible for binding acetylated lysine in histone tails, we reasoned that histone acetylation mediates the interaction between the WSTF bromodomain and HeLa histone octamers. This idea was supported by the observed *in vitro* association between the WSTF bromodomain and histone octamers, which was indeed abrogated when histone octamers were deacetylated using anti-FLAG immunoprecipitates (Figure 5B, odd number lanes).

To determine whether the histone acetylation was sufficient to promote this interaction, we established an *in vitro* histone binding assay using recombinant histone octamers. The integrity and HAT activity of purified recombinant p300 were assessed by CBB stain of the protein and *in vitro* acetylation of recombinant histone octamers (Figure 5C). The WSTF bromodomain bound to recombinant histone octamers only when the histones were acetylated (Figure 5D). We then further analyzed selective recognition of acetylated lysine residues in histone N-terminal tails by WSTF. Among biotin-conjugated tail peptides, WSTF selectively recognized some of the known acetylated lysine residues, histone AcH2BK12, AcH3K14, AcH4K16. However, ablation of the WSTF bromodomain (WSTFΔC) resulted in loss of the WSTF interaction with acetylated histones (Figure 5E). Our results thus suggested that the WSTF C-terminal region selectively associated with post-translationally acetylated lysine residues in the histone tails through the WSTF bromodomain.

Physical interactions between the WSTF C-terminal region and acetylated histones are required for the ligand-induced transrepression of the 1α(OH)ase gene

We next examined the role of WSTF in binding to acetylated histones during VDR-mediated gene repression. A WSTFΔC construct was first assessed in MCF7 cells by immunoprecipitation using anti-FLAG antibodies and Western blotting with anti-acetylated lysine 14 of histone H3 (AcH3K14), anti-acetylated histone H3 (AcH3), anti-Brg1 and anti-VDR antibodies. Both WT WSTF and the WSTFΔC mutant appeared to associate with VDR and Brg1, which is an ATPase subunit of WINAC, as well as the other SWI/SNF chromatin-remodeling complex subtypes. However, the WSTFΔC mutant exhibited no clear association with AcH3 and AcH3K14 (Figure 6A). These findings imply that the highly acetylated state of histones induces a stable association between WSTF and chromatin *in vivo*.

To further characterize this association, a ChIP assay was performed. TSA treatment potentiated histone H3 and H3K14 acetylation around 1αnVDRE (nVDRE), as expected, with increased recruitment of VDR and WSTF (Figure 6B, left panel). In the distal region of the 1α(OH)ase gene promoter, histone H3 acetylation was partially enhanced by TSA, though WSTF, VDR or VDIR was undetectable. As expected from the previous findings of $1\alpha,25(OH)_2D_3$-induced recruitment of HDAC to 1αnVDRE via VDIR/VDR (Murayama *et al*, 2004), $1\alpha,25(OH)_2D_3$ treatment caused clear deacetylation of histone H3 around 1αnVDRE. The WSTFΔC mutant was again unable to associate with the 1αnVDRE region, regardless of the hyperacetylated state of histone H3 (Figure 6B, right panel). A reporter assay using the luciferase gene driven by the 1α(OH)ase promoter showed that WSTF expression potentiated the $1\alpha,25(OH)_2D_3$-induced transrepression along with Brg1 (Figure 6C), whereas the WSTFΔC mutant acted as a dominant-negative factor in terms of the ligand-induced transrepression (Figure 6C, black bars). Thus, it appears that WSTF interacts with acetylated histones via the bromodomain *in vivo*, and that this interaction is indispensable for VDR-mediated transrepression through 1αnVDRE.

Discussion

Role of WINAC in the ligand-dependent corepressor recruitment

Transcription control by NRs encompasses multiple steps with the help of a large number of coregulator complexes (Glass and Rosenfeld, 2000; McKenna and O'Malley, 2002). ATP-dependent chromatin-remodeling complexes are considered to support the promoter-specific recruitment of other coregulator complexes (Emerson, 2002; Narlikar *et al*, 2002). We have previously reported that the WINAC dysfunction resulted in a failure of proper transcriptional regulation by

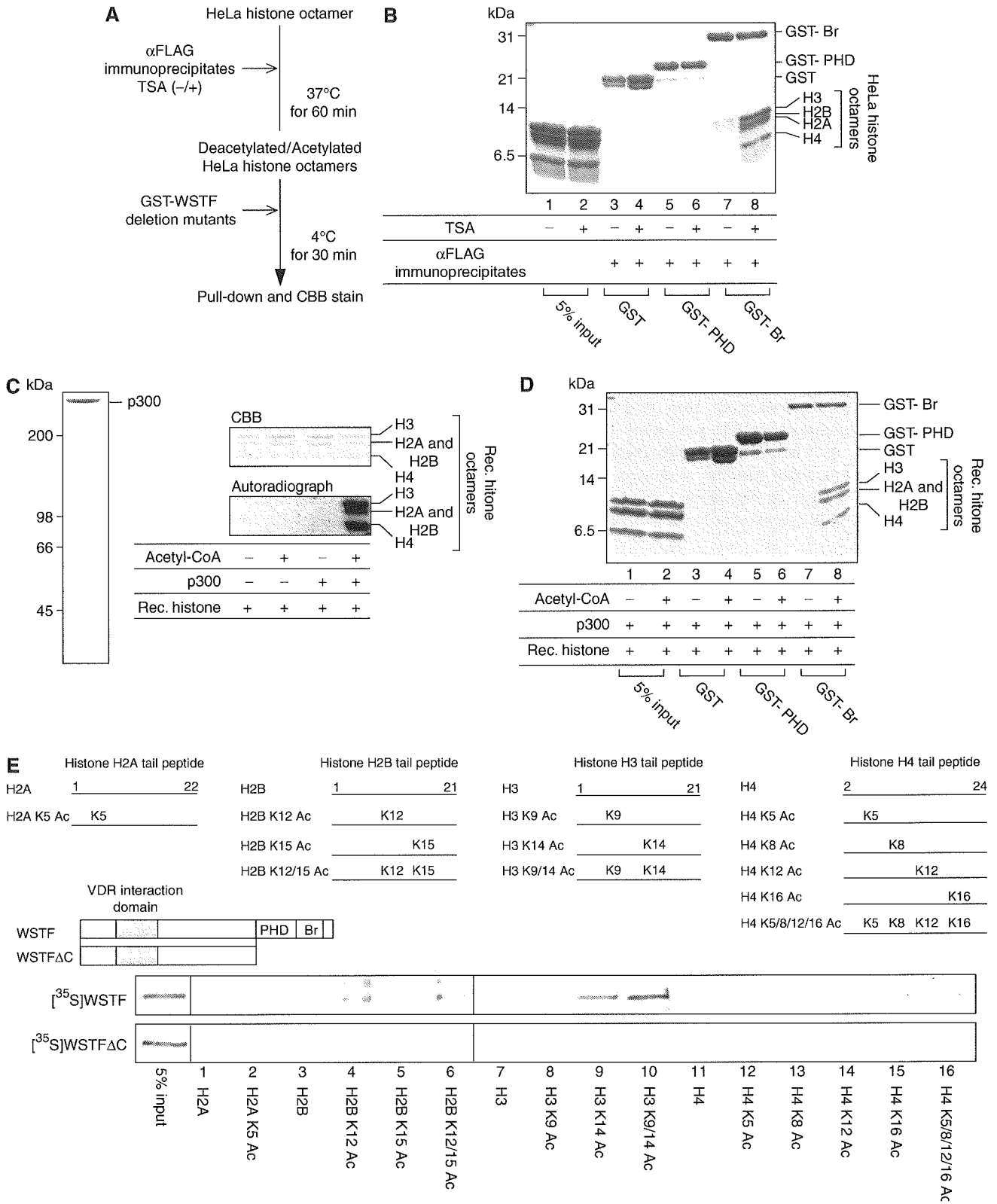

VDR, possibly because of impairment of coregulator recruitment to VDR target gene promoter. These findings strongly suggested that ATP-dependent chromatin-remodeling activity is indispensable for subsequent coregulator recruitment in response to ligand binding. However, the molecular mechanism in ligand-induced transrepression has not been well understood.

It has been considered that ligand-unbound VDR/RXR on VDRE mainly associates with HDAC complex to actively repress target genes. Reflecting this model, ligand binding led to corepressor dissociation from VDR (Figure 2A). In contrast, we also showed that WINAC assisted promoter recruitment of HDAC corepressor complex in VDIR-mediated transrepression on a negative VDRE (Figure 3A). These results may indicate a difference in the set of associating factors/complexes with unliganded VDR on negative VDREs from positive VDREs on the VDR target gene promoters. Indeed, ligand binding significantly increases the interaction of VDR/WINAC with HDAC complex (Figure 2A and B). A WSTF mutant with a deleted C-terminal region containing bromodomains functions as a dominant-negative mutant in terms of ligand-induced transrepression by VDR (Figure 6C), although this mutant could interact with VDR (Figure 6A). Moreover, this mutant abrogated ligand-dependent histone deacetylation, considering loss of acetylated histone recognition and subsequent HDAC corepressor recruitment. Hence, in addition to ligand-induced transactivation by VDR, WINAC has an important role in VDR-mediated transrepression mechanism. The proposed mechanism of the ligand-induced transrepression by VDR in the present study appears to be dependent on the promoter content, since it is unlikely that all of the VDR target gene promoters for vitamin D-induced transrepression harbor VDIR binding sites. The other mode and mechanism of ligand-induced transrepression might be unrevealed in the other promoters for VDR and the other NRs.

Promoter targeting of VDR requires chromatin structures

In this report, we investigated the role of WINAC in the recruitment of VDR to 1αnVDRE in the 1α(OH)ase gene promoter with consequent ligand-induced transrepression. We showed *in vitro* that WINAC potentiated association of VDR with 1αnVDRE, irrespective of the ligand binding, when the promoter DNA was configured as a nucleosome array (Figure 4). In contrast, in naked DNA fragments, only liganded VDR was recruited to 1αnVDRE via association with VDIR. Moreover, biochemical mapping experiments demonstrated that the WSTF bromodomain has an interaction surface with histone octamers (Figure 5B and E). These results suggest that WINAC aids promoter occupancy by unliganded VDR, acting as a tether between VDR and promoter nucleosomal arrays. This model was further supported by the *in vivo* observation that a decrease in WSTF levels due to RNAi expression attenuated VDR retention on the endogenous 1α(OH)ase gene promoter (Figure 3A). As VDR directly interacts with WSTF in a ligand-independent manner, VDR could be targeted to the promoter irrespective of ligand binding through its association with WSTF.

Transition from the transactivation state to the transrepression state

1α(OH)ase gene expression is induced by calciotropic peptide hormones such as parathyroid hormone (PTH) (Brenza *et al*, 1998; Murayama *et al*, 1998). It has been previously shown that VDIR is phosphorylated by PKA as a downstream effect of PTH activity, which then leads to HAT p300/CBP complex binding and transactivation (Murayama *et al*, 2004). The recruited HAT coactivator complex is presumed to acetylate the nucleosomal array around 1αnVDRE, and consequently this acetylation renders the 1α(OH)ase promoter accessible to the 1α,25$(OH)_2D_3$-unbound VDR/WINAC complex. Furthermore, the weak interaction between unliganded VDR and VDIR, shown in Figure 3B, uncovered the existence of this transition stage (see Figure 7). In this study, we show that a WSTF mutant with a deletion of the C-terminal region, which includes bromodomains, abolished the retention of the WINAC complex on the acetylated 1α(OH)ase gene promoter. This deletion mutant also functions as a dominant-negative form of WSTF to carry out ligand-induced transrepression (Figure 6). These results indicate that assembly of these factors prior to ligand binding is indispensable to initiate ligand-induced transrepression. Upon VDR binding to 1α,25$(OH)_2D_3$, VDR stably associates with VDIR, leading to recruitment of the HDAC corepressor complex with the assistance of WINAC chromatin-remodeling activity. Alternatively, it is also possible to presume that WINAC stabilizes the association of VDR with the HDAC corepressor complex. In any case, ligand binding to VDR results in transcriptional repression of these gene expressions through DNA-bound VDIR and the WINAC complex.

Several pieces of evidence support our finding of a physical interaction between acetylated histones and ATP-dependent

Figure 5 WSTF bromodomains in its C-terminal region interact with acetylated histone octamers. (**A**) Schematic diagram of a histone binding assay. HDAC immunoprecipitate was prepared using an anti-FLAG antibody from whole-cell extracts of 1α,25$(OH)_2D_3$-treated MCF7 cells transiently expressing FLAG-WSTF (see Figure 2B). (**B**) An *in vitro* histone binding assay showed that the interaction between WSTF bromodomains and HeLa histone octamers is decreased after deacetylation of the HeLa histone octamers. HeLa histone octamers were incubated with HDAC complexes, mixed with GST-fused WSTF bromodomain and PHD finger regions and then immobilized onto glutathione-Sepharose beads. Bound materials were eluted from the resin and resolved by 18% SDS–PAGE. Proteins were visualized by CBB staining. (**C**) SDS–PAGE analysis of recombinant p300 and *in vitro* histone acetylation of recombinant histone octamers. Affinity-tagged recombinant p300 was expressed in Sf9 cells using a baculovirus system and purified by affinity chromatography as described in Materials and methods. Histone octamers were acetylated *in vitro* by p300 with radiolabeled acetyl-CoA and the gels were visualized by CBB staining following exposure to film. (**D**) Interaction between recombinant histone octamers and WSTF bromodomains is enhanced after *in vitro* histone acetylation by p300. Recombinant histone octamers were preincubated with p300 in the absence (upper panel) or presence (lower panel) of acetyl-CoA and subjected to histone binding assay. (**E**) Site-specific recognition between the WSTF bromodomain and histones with tail modification. Schematic diagrams of the WSTF deletion mutants used are illustrated (upper panel). ^{35}S-labeled WSTF and a WSTFΔC mutant translated *in vitro* were incubated with a series of acetylated N-terminal histone tails immobilized onto streptavidin beads. Histone tail peptides were tested for WSTF binding (middle panel). Bound WSTF was resolved by SDS–PAGE, followed by autoradiography (lower panel).

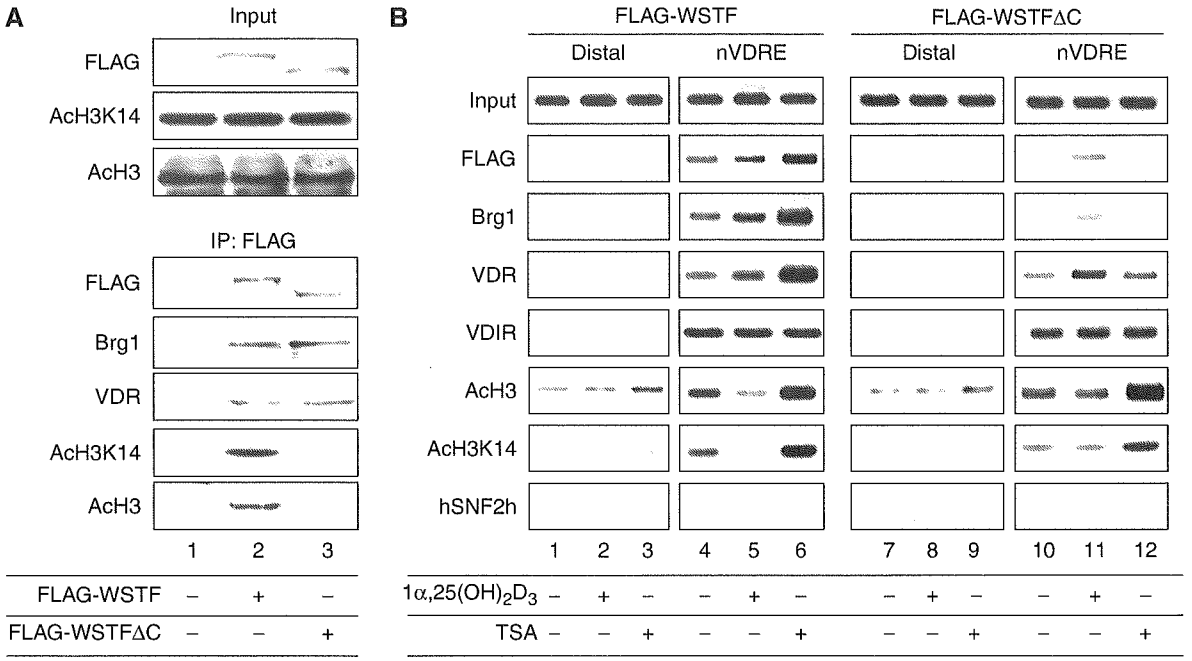

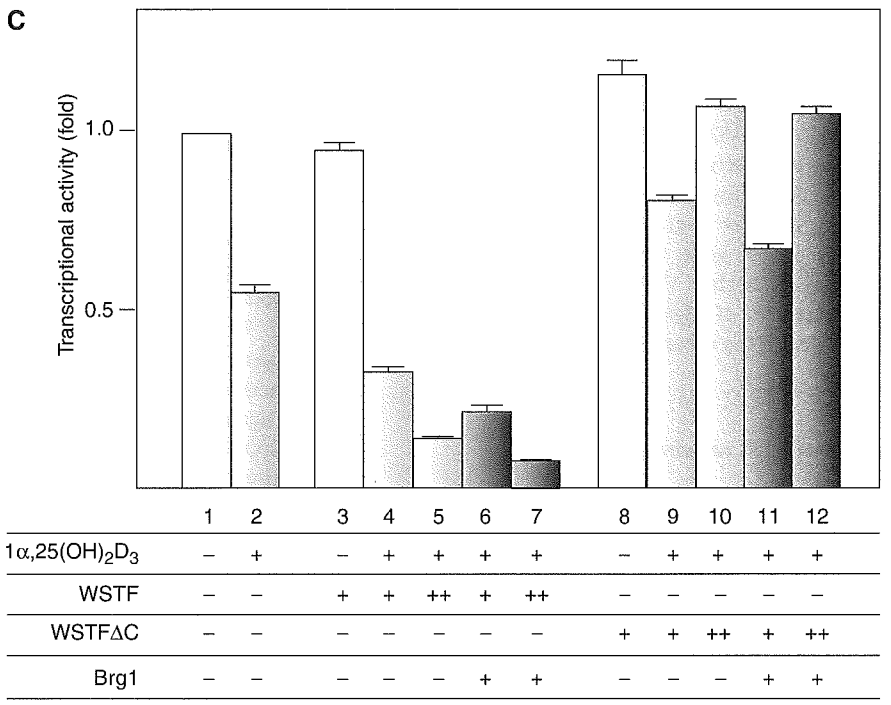

Figure 6 The WSTF C-terminal region is indispensable for the promoter targeting of ligand-unbound VDR and for VDR-mediated transrepression of the 1α(OH)ase gene. (**A**) WSTFΔC shows no binding to acetylated histone H3. MCF7 cells transfected with FLAG-tagged WSTF, FLAG-tagged WSTFΔC or pcDNA3 vector as a control were lysed and subjected to immunoprecipitation with anti-FLAG. Immunoprecipitates were Western blotted with indicated antibodies (lower panel). (**B**) Histone acetylation-dependent recruitment of WSTF to the 1αnVDRE region. MCF7 cells transfected with FLAG-tagged WSTF or FLAG-tagged WSTFΔC were treated with either $1\alpha,25(OH)_2D_3$ (10^{-8} M) for 45 min or TSA (10^{-7} M) for 120 min and then subjected to ChIP analysis. (**C**) A WSTF mutant with a deleted C-terminal bromodomain and PHD finger (WSTFΔC) exerted a partial dominant-negative effect on the ligand-induced transrepression function of VDR. The amounts of each transfected plasmid are described in Figure 1A.

chromatin-remodeling complexes. For instance, histone acetylation by Gcn5 has been shown to recruit SWI/SNF complexes during activation of the interferon-β promoter (Agalioti *et al*, 2000). Likewise, ligand-induced transactivation by RAR/RXR also requires histone acetylation prior to chromatin remodeling by SWI/SNF complexes *in vitro* (Dilworth *et al*, 2000). However, all of these studies focused on the role of histone acetylation in transcriptional activation. Thus, we have revealed a novel mechanism by which histone acetylation may be linked with transcriptional repression, even though the acetylation of nucleosomes is generally considered to enhance eukaryotic gene expression.

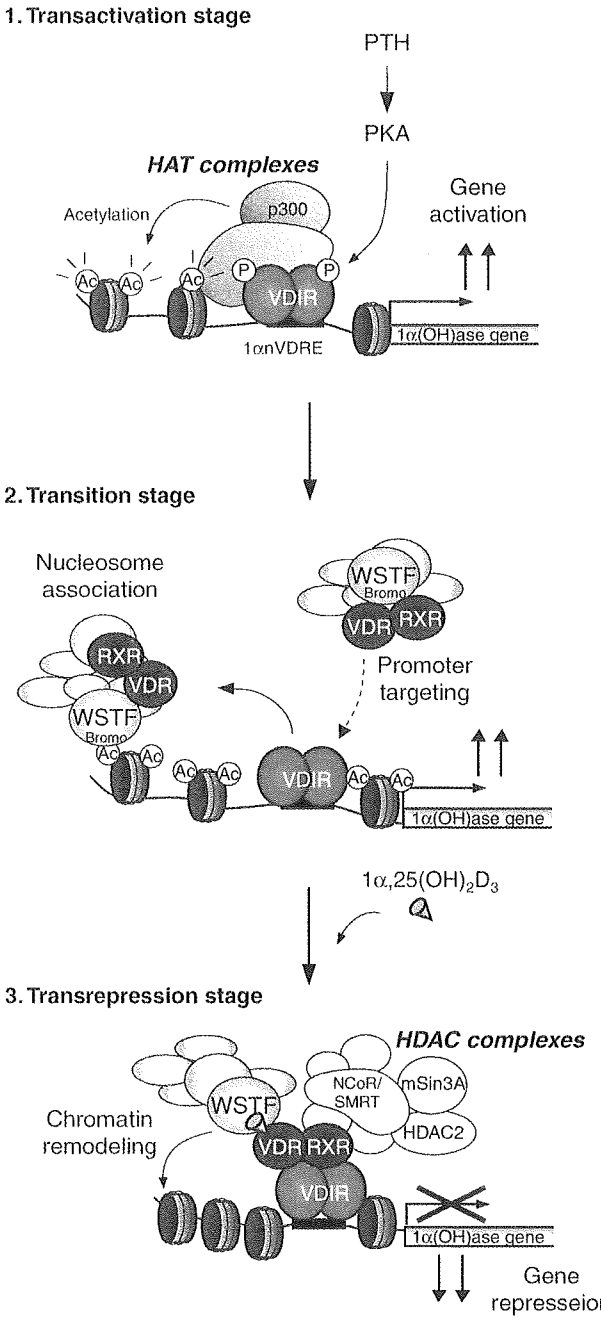

Figure 7 Model demonstrating the role of WINAC in the ligand-induced transrepression function of VDR at the 1α(OH)ase gene promoter. p300 is recruited to VDIR, which was phosphorylated via PKA signaling, and it acetylates the nucleosomes around the 1α(OH)ase gene promoter region (transactivation stage). WINAC, along with VDR, sequentially targets VDIR through interaction between unliganded VDR and VDIR, and is retained on the acetylated promoter via the WSTF bromodomain. VDR becomes receptive to $1\alpha,25(OH)_2D_3$ binding (transition stage). Upon $1\alpha,25(OH)_2D_3$ binding, HDAC corepressor complexes are recruited to the ligand-bound VDR/VDIR complex, and they then deacetylate the nucleosomes. WINAC then exerts its ATP-dependent chromatin-remodeling activity (transrepression stage).

VDR/WINAC targets VDIR on 1αnVDRE and anchors on the promoter via a physical interaction between the WSTF bromodomain and acetylated histones

In this report, we showed that the WSTF bromodomain physically interacts with acetylated histone octamers *in vitro* (Figure 5), and that the WSTF bromodomain is indispensable for ligand-induced transrepression by VDR (Figure 6). Physical interaction of acetylated histones with the bromodomains harbored in ATP-dependent chromatin-remodeling complex components is considered to be a critical step in the activation of chromatin, modulating its architecture by rearrangement of nucleosome arrays (Winston and Allis, 1999; Jones *et al*, 2000). Hassan *et al* (2002) found that both the SAGA and SWI/SNF complexes are capable of anchoring to promoter nucleosomes through direct contact of acetylated histones with the bromodomains. However, it remained unclear how these chromatin-remodeling complexes selectively discriminate their target chromosomal areas from others through their chromatin recognition modules. To address this point, we have examined two aspects of WINAC promoter targeting. One is the mechanism by which specific chromatin areas are recognized by WSTF through association with sequence-specific regulators, and the other is the preference of WSTF for a specific chromatin condition.

To address the first aspect of WINAC promoter targeting, we investigated the role of VDR by using $VDR^{-/-}$ MEF cells. Our experiments showed *in vivo* that WSTF recruitment to the 1α(OH)ase promoter was significantly impaired in $VDR^{-/-}$ MEF cells, even though the acetylation level of histones and VDIR occupancy in the promoter were unchanged when compared to WT MEF cells (Figure 3D). These results suggested that the association between the WSTF bromodomain and acetylated nucleosomes itself is not stable enough to anchor the VDR/WINAC complex on the promoters. Indeed, clear VDR/WSTF retention on the chromatin templates required VDIR bound to 1αnVDRE (Figure 4F, lanes 11 and 12). Previous reports have shown that SWI/SNF complexes are able to associate with promoter nucleosomes, but the association was somewhat unstable on an unmodified nucleosomal array (Cote *et al*, 1998). Therefore, ATP-dependent chromatin-remodeling complexes may require a physical interaction with the sequence-specific regulators to maintain their promoter occupancy. In this respect, VDIR could be considered as a hallmark for targeting of VDR/WINAC to the specific chromosomal areas.

The second aspect of WINAC promoter targeting was addressed by showing a preferential interaction of WSTF with acetylated amino-acid residues in histones. Acetylation of lysines on the histone tails is thought to establish a distinct histone code that directs molecular processes, including gene regulation (Strahl and Allis, 2000). A number of factors have turned out to harbor bromodomains, and these are believed to utilize diverse histone codes to carry out different cellular functions. We found that the WSTF bromodomain preferentially binds to acetylated Lys^{14} of histone H3 (Figure 5F). This lysine residue is considered to be the best HAT substrate for p300, as a previous study showed that p300 effectively acetylates Lys^{14} in histone H3 in a nucleosomal context (Schiltz *et al*, 1999; Lau *et al*, 2000). Together with our previous findings that p300/CBP is a HAT coactivator for VDIR bound to 1αnVDRE, this suggests that interaction of the WSTF bromodomain with acetylated H3 Lys^{14} by p300 enables WINAC to discriminate, at least to some extent, the target promoter regions from other nonspecific acetylated regions.

Thus, considering all of these results, we conclude that WINAC facilitates VDR-mediated transrepression of the

1α(OH)ase gene through a physical interaction between the WSTF bromodomain and an acetylated nucleosomal array. This mechanism is likely indispensable for the biological functions of the VDR, such as a negative feedback control in the $1\alpha,25(OH)_2D_3$ biosynthesis pathway.

Materials and methods

Plasmids and RNAi

For transfection studies, the two 1αnVDRE sequences (5′-CAT TTT AGC CCA TTA ACC CAC CTG CCA TCT GCC C-3′) and the 1α(OH)ase promoter (nucleotides −615 to −60 relative to the RNA start site) were inserted into the pGL3-Luciferase vector (Promega) under the control of a TATA promoter. Expression vectors for full-length rat VDR, rat RXR and human FLAG-tagged WSTF were as previously described (Kitagawa *et al*, 2003). Full-length mouse VDIR cDNA tagged with 6 × His was inserted into pcDNA3 (Invitrogen). cDNA encoding a human WSTF deletion mutant (amino acids 1–1185, WSTFΔC) N-terminally tagged with FLAG was cloned into pcDNA3. A series of human WSTF deletion mutants fused with GST were cloned into pGEX-4T (Pharmacia) (Kitagawa *et al*, 2003). For an immobilized template recruitment assay, the human 1α(OH)ase promoter distal region (nucleotides −3615 to −3060 relative to the RNA start site) was cloned into the pGL3 vector.

The two short RNA oligomers denatured at 90°C were annealed for 1 h at 60°C (Kitagawa *et al*, 2003). The RNAi sequences used were as follows: WSTF (5′-GAG UAU GAA GCC CGC UUG GTT-3′ and 5′-CCA AGC GGG CUU CAU ACU CTT-3′); VDR (5′-UCA AUG CUA UGA CCU GUG AUU-3′ and 5′-UCA CAG GUC AUA GCA UUG AUU-3′); VDIR (5′-GAA CCU GAA UCC CAA AGC AUU-3′ and 5′-UGC UUU GGG AUU CAG GUU CUU-3′); lamin A/C Duplex (as a control; Dharmacon) (5′-CUG GAC UUC CAG AAG AAC ATT-3′ and 5′-TTG ACC UGA AGG UCU UCU UGU-3′).

Protein purification

HeLa histone octamers were prepared from HeLa nuclear pellets as previously described (Hassan *et al*, 2002). HeLa cells (3 l culture) were lysed in lysis buffer (20 mM HEPES, pH 7.5, 0.25 M sucrose, 3 mM $MgCl_2$, 0.2% Nonidet-P40 (NP-40), 3 mM 2-mercaptoethanol, 0.4 mM PMSF, 1 μM pepstatin A and 1 μM leupeptin) by Dounce homogenization with pestle B. After washing the pellet with buffer B (20 mM HEPES, pH 7.5, 3 mM $MgCl_2$, 0.2 mM EGTA, 3 mM 2-mercaptoethanol, 0.4 mM PMSF, 1 μM pepstatin A and 1 μM leupeptin), nuclear proteins were extracted with buffer B containing 0.3 M KCl and 5% glycerol. The nuclear pellets were resuspended in HAP buffer (50 mM sodium phosphate, pH 6.8, 0.6 M NaCl, 1 mM 2-mercaptoethanol and 0.5 mM PMSF). To remove extra DNA fragments and histone H1, 20 g of dry BioGel HTP powder (Bio-Rad) was added to the suspension and the slurries were poured into a column (2.5 × 20 cm). After washing the resin extensively with HAP buffer, HeLa histone octamers were eluted with HAP buffer containing 2.5 M NaCl. Purified histone octamers were concentrated using Centriprep-3 (Amicon).

Recombinant *Xenopus* histones (H2A, H2B, H3, H4) were expressed and purified as previously described (Luger *et al*, 1999; Dyer *et al*, 2004). Recombinant p300, dNAP1 and dACF complexes were prepared essentially as described previously (Ito *et al*, 1997; Dilworth *et al*, 2000; Nakagawa *et al*, 2001). Briefly, His_6-tagged p300 and His_6-tagged dNAP1 were purified from baculovirus-infected Sf9 cells using Ni-NTA resin (Qiagen), followed by conventional anion exchange chromatography using SOURCE 15Q (Pharmacia) for dNAP1. Recombinant dACF complexes were prepared from Sf9 cells infected with baculovirus vectors encoding dACF complex components, FLAG-tagged dAcf-1 and dISWI, by affinity chromatography using anti-FLAG M2 agarose (Sigma). All proteins were dialyzed against HEG buffer (HEPES, pH 7.6, 1 mM EDTA, 10% glycerol, 0.15 M NaCl, 1 mM DTT and 0.5 mM PMSF), and protein concentrations were evaluated by SDS–PAGE and visualized with CBB R-250, using BSA as a standard.

Establishment and maintenance of WT and VDR$^{-/-}$ MEF cell lines

MEF cell lines were obtained from WT or $VDR^{-/-}$ 13.5-day-old embryos and used at the 10th generation (Ito *et al*, 2000). The MEF cell lines were replated at a density of 1×10^6 cells on gelatin-coated 10-cm dishes and maintained in DMEM supplemented with 10% FBS at 37°C in 5% CO_2.

Immunoprecipitation

After washing MCF7 cells with ice-cold PBS, cells were collected and resuspended in 100 μl lysis buffer (20 mM Tris–HCl, pH 7.9, 1% NP-40, 1 mM EDTA, 150 mM NaCl, 2.5 mM $MgCl_2$, 5% glycerol, 5 mM DTT, 10 μg/ml aprotinin and 1 mM PMSF) containing 0.1% SDS, incubated on ice for 30 min and then centrifuged for 30 min at 12 000 *g*. After centrifugation, the supernatants were diluted 10 times with lysis buffer and used as MCF7 whole-cell extracts for immunoprecipitation using anti-FLAG (Sigma), anti-VDR (Neomarkers), anti-WSTF (Cell signaling) or anti-VDIR (Santa Cruz) antibodies (Yanagisawa *et al*, 2002; Kitagawa *et al*, 2003; Murayama *et al*, 2004).

ChIP and Re-ChIP assay

ChIP analysis was performed using the ChIP assay kit (Upstates) (Yanagisawa *et al*, 2002; Kitagawa *et al*, 2003), according to the manufacturer's instructions. Intact MCF7 cells or transfected cells, and WT or $VDR^{-/-}$ MEF cells were cultured in the presence of ligand. Soluble chromatin prepared from 1×10^6 cells was immunoprecipitated with antibodies against the indicated proteins, including anti-NCoR (Alexis), anti-AcH3 (Upstates) or hSNF2h (Santa Cruz) as a negative control.

Immobilized DNA/chromatin template recruitment assays

Recruitment assays were performed as previously described (Hassan *et al*, 2002). The 1α(OH)ase promoter or distal fragment was cleaved from the 1α(OH)ase promoter/pGL3 or 1a(OH)ase distal region/pGL3 with *Mlu*I and *Bgl*II, end-labeled with biotin-14-dATP (Gibco) and gel purified. The fragments (0.2 μg DNA) were then reconstituted as chromatin with purified HeLa histone octamers (0.15 μg), recombinant histone octamers (0.3 μg), purified recombinant dNAP1 (2.5 μg), and purified recombinant dACF complexes (10 ng) and ATP (5 mM; Sigma) as described previously (Kitagawa *et al*, 2003). Biotinylated DNA or nucleosomal arrays were incubated at room temperature for 1 h with paramagnetic beads coupled to streptavidin (Dynabeads streptavidin, Dynal) in binding buffer (10 mM Tris–HCl, pH 7.9, 0.3 M KCl, 5 mM DTT, 5 mM PMSF, 5% glycerol and 0.25 mg/ml BSA) and washed extensively with binding buffer supplemented with 0.5 M KCl. Whole-cell extracts, prepared from three 75 cm^3 dishes of MCF-7 cells stably expressing FLAG-hWSTF treated with or without 10^{-8} M $1\alpha,25(OH)_2D_3$, were preincubated with 1 μg of circular competitor chromatin for 30 min and then added to the prepared templates and further incubated in lysis buffer for 1 h at 37°C. Either 100 pmol of double-stranded 1αnVDRE-oligo (5′-TAA CCC ACC TGC CAT CTG CCC AGT-3′) as a competitor or 100 pmol of double-stranded DR5-oligo (5′-TAA GGG TTC ACC GAA AGT TCA CTC GCA T-3′) as a control was then added and samples were further incubated for 1 h at 30°C. Subsequently, templates were concentrated using a magnet and washed twice in binding buffer containing 50 mM KCl before being used in Western blot analysis.

In vitro histone acetylation and histone deacetylation

For *in vitro* histone acetylation experiments, recombinant histone octamers (0.5 μg) were incubated with or without recombinant p300 (200 ng) in HEG buffer. Acetyl-CoA mix (1 μM radiolabeled and 9 μM cold acetyl-CoA) was then added and histone acetylation was carried out at 30°C for 30 min. After stopping the reaction by incubating on ice for 30 min, samples were analyzed on an 18% SDS–PAGE gel, which was visualized with Coomassie staining before immersion in Enhance (NEN) fluorography reagent as the manufacturer's instructions. The gel was then dried and visualized by autoradiography.

For *in vitro* histone deacetylation, anti-FLAG immunoprecipitates were prepared from whole extracts of MCF7 cells transfected with empty pcDNA3 vector or FLAG-WSTF/pcDNA3 and cultured with or without 10^{-8} M $1\alpha,25(OH)_2D_3$ for 48 h. HDAC activity of the immunoprecipitates was measured using an HDAC assay kit (Fluorometric detection, Upstate Biotech.) according to the manufacturer's instructions. HeLa histone octamers were deacetylated by incubation with immunoprecipitates containing HDAC activity in the presence or absence of 10^{-6} M TSA at 37°C for 60 min.

Peptide binding assay

Peptide binding assay was performed as previously reported (Dey *et al*, 2003). Briefly, ^{35}S-labeled proteins translated *in vitro* were incubated with 2 μg of biotin-labeled synthetic peptides corresponding to the N-terminal tails of histone H2A, H2B, H3 and H4 (purchased from Upstate, or synthesized from Genemed Synthesis) in a binding buffer (50 mM Tris–HCl (pH 7.5), 15 mM $MgCl_2$, 150 mM NaCl, 0.5 mM DTT and 0.1% NP-40) for 2 h at 4°C, followed by incubation with 20 μl of M-280 streptavidin beads (Dynal). Bound materials were subjected to SDS–PAGE, followed by autoradiography.

Acknowledgements

We thank Dr Timothy J Richmond for kindly providing the xHistone expression vector, Dr JT Kadonaga for the recombinant baculovirus expressing human p300 and Dr K Luger for technical discussions. We also thank Mr Y Mezaki and Dr AP Kouzmenko for technical support, and Ms H Higuchi for manuscript preparation. This work was supported in part by a grant-in-aid for Basic Research Activities for Innovative Biosciences (BRAIN) and priority areas from the Ministry of Education, Science, Sports, and Culture of Japan (to SK).

References

Agalioti T, Lomvardas S, Parekh B, Yie J, Maniatis T, Thanos D (2000) Ordered recruitment of chromatin modifying and general transcription factors to the IFN-beta promoter. *Cell* **103:** 667–678

Brenza HL, Kimmel-Jehan C, Jehan F, Shinki T, Wakino S, Anazawa H, Suda T, DeLuca HF (1998) Parathyroid hormone activation of the 25-hydroxyvitamin D3-1alpha-hydroxylase gene promoter. *Proc Natl Acad Sci USA* **95:** 1387–1391

Cote J, Peterson CL, Workman JL (1998) Perturbation of nucleosome core structure by the SWI/SNF complex persists after its detachment, enhancing subsequent transcription factor binding. *Proc Natl Acad Sci USA* **95:** 4947–4952

Dey A, Chitsaz F, Abbasi A, Misteli T, Ozato K (2003) The double bromodomain protein Brd4 binds to acetylated chromatin during interphase and mitosis. *Proc Natl Acad Sci USA* **100:** 8758–8763

Dhalluin C, Carlson JE, Zeng L, He C, Aggarwal AK, Zhou MM (1999) Structure and ligand of a histone acetyltransferase bromodomain. *Nature* **399:** 491–496

Dilworth FJ, Fromental-Ramain C, Yamamoto K, Chambon P (2000) ATP-driven chromatin remodeling activity and histone acetyltransferases act sequentially during transactivation by RAR/RXR *in vitro*. *Mol Cell* **6:** 1049–1058

Dyer PN, Edayathumangalam RS, White CL, Bao Y, Chakravarthy S, Muthurajan UM, Luger K (2004) Reconstitution of nucleosome core particles from recombinant histones and DNA. *Methods Enzymol* **375:** 23–44

Emerson BM (2002) Specificity of gene regulation. *Cell* **109:** 267–270

Fyodorov DV, Kadonaga JT (2001) The many faces of chromatin remodeling: SWItching beyond transcription. *Cell* **106:** 523–525

Glass CK, Rosenfeld MG (2000) The coregulator exchange in transcriptional functions of nuclear receptors. *Genes Dev* **14:** 121–141

Gu W, Malik S, Ito M, Yuan CX, Fondell JD, Zhang X, Martinez E, Qin J, Roeder RG (1999) A novel human SRB/MED-containing cofactor complex, SMCC, involved in transcription regulation. *Mol Cell* **3:** 97–108

Hassan AH, Prochasson P, Neely KE, Galasinski SC, Chandy M, Carrozza MJ, Workman JL (2002) Function and selectivity of bromodomains in anchoring chromatin-modifying complexes to promoter nucleosomes. *Cell* **111:** 369–379

Heinzel T, Lavinsky RM, Mullen TM, Soderstrom M, Laherty CD, Torchia J, Yang WM, Brard G, Ngo SD, Davie JR, Seto E, Eisenman RN, Rose DW, Glass CK, Rosenfeld MG (1997) A complex containing N-CoR, mSin3 and histone deacetylase mediates transcriptional repression. *Nature* **387:** 43–48

Ito M, Yuan CX, Okano HJ, Darnell RB, Roeder RG (2000) Involvement of the TRAP220 component of the TRAP/SMCC coactivator complex in embryonic development and thyroid hormone action. *Mol Cell* **5:** 683–693

Ito T, Bulger M, Pazin MJ, Kobayashi R, Kadonaga JT (1997) ACF, an ISWI-containing and ATP-utilizing chromatin assembly and remodeling factor. *Cell* **90:** 145–155

Jacobson RH, Ladurner AG, King DS, Tjian R (2000) Structure and function of a human TAFII250 double bromodomain module. *Science* **288:** 1422–1425

Jones MH, Hamana N, Nezu J, Shimane M (2000) A novel family of bromodomain genes. *Genomics* **63:** 40–45

Kamei Y, Xu L, Heinzel T, Torchia J, Kurokawa R, Gloss B, Lin SC, Heyman RA, Rose DW, Glass CK, Rosenfeld MG (1996) A CBP integrator complex mediates transcriptional activation and AP-1 inhibition by nuclear receptors. *Cell* **85:** 403–414

Kato S, Fujiki R, Kitagawa H (2004) Vitamin D receptor (VDR) promoter targeting through a novel chromatin remodeling complex. *J Steroid Biochem Mol Biol* **89-90:** 173–178

Kitagawa H, Fujiki R, Yoshimura K, Mezaki Y, Uematsu Y, Matsui D, Ogawa S, Unno K, Okubo M, Tokita A, Nakagawa T, Ito T, Ishimi Y, Nagasawa H, Matsumoto T, Yanagisawa J, Kato S (2003) The chromatin-remodeling complex WINAC targets a nuclear receptor to promoters and is impaired in Williams syndrome. *Cell* **113:** 905–917

Lau OD, Kundu TK, Soccio RE, Ait-Si-Ali S, Khalil EM, Vassilev A, Wolffe AP, Nakatani Y, Roeder RG, Cole PA (2000) HATs off: selective synthetic inhibitors of the histone acetyltransferases p300 and PCAF. *Mol Cell* **5:** 589–595

Lemon B, Inouye C, King DS, Tjian R (2001) Selectivity of chromatin-remodelling cofactors for ligand-activated transcription. *Nature* **414:** 924–928

Luger K, Rechsteiner TJ, Richmond TJ (1999) Preparation of nucleosome core particle from recombinant histones. *Methods Enzymol* **304:** 3–19

Mangelsdorf DJ, Thummel C, Beato M, Herrlich P, Schutz G, Umesono K, Blumberg B, Kastner P, Mark M, Chambon P, Evans RM (1995) The nuclear receptor superfamily: the second decade. *Cell* **83:** 835–839

McKenna NJ, O'Malley BW (2002) Combinatorial control of gene expression by nuclear receptors and coregulators. *Cell* **108:** 465–474

Murayama A, Kim MS, Yanagisawa J, Takeyama KI, Kato S (2004) Transrepression by a liganded nuclear receptor via a bHLH activator through co-regulator switching. *EMBO J* **23:** 1598–1608

Murayama A, Takeyama K, Kitanaka S, Kodera Y, Hosoya T, Kato S (1998) The promoter of the human 25-hydroxyvitamin D3 1 alpha-hydroxylase gene confers positive and negative responsiveness to PTH, calcitonin, and 1 alpha,25(OH)2D3. *Biochem Biophys Res Commun* **249:** 11–16

Nakagawa T, Bulger M, Muramatsu M, Ito T (2001) Multistep chromatin assembly on supercoiled plasmid DNA by nucleosome assembly protein-1 and ATP-utilizing chromatin assembly and remodeling factor. *J Biol Chem* **276:** 27384–27391

Narlikar GJ, Fan HY, Kingston RE (2002) Cooperation between complexes that regulate chromatin structure and transcription. *Cell* **108:** 475–487

Onate SA, Tsai SY, Tsai MJ, O'Malley BW (1995) Sequence and characterization of a coactivator for the steroid hormone receptor superfamily. *Science* **270:** 1354–1357

Rachez C, Suldan Z, Ward J, Chang CP, Burakov D, Erdjument-Bromage H, Tempst P, Freedman LP (1998) A novel protein complex that interacts with the vitamin D3 receptor in a ligand-dependent manner and enhances VDR transactivation in a cell-free system. *Genes Dev* **12:** 1787–1800

Schiltz RL, Mizzen CA, Vassilev A, Cook RG, Allis CD, Nakatani Y (1999) Overlapping but distinct patterns of histone acetylation by the human coactivators p300 and PCAF within nucleosomal substrates. *J Biol Chem* **274:** 1189–1192

Strahl BD, Allis CD (2000) The language of covalent histone modifications. *Nature* **403:** 41–45

Takeyama K, Kitanaka S, Sato T, Kobori M, Yanagisawa J, Kato S (1997) 25-Hydroxyvitamin D3 1alpha-hydroxylase and vitamin D synthesis. *Science* **277:** 1827–1830

Winston F, Allis CD (1999) The bromodomain: a chromatin-targeting module? *Nat Struct Biol* **6:** 601–604

Yanagisawa J, Kitagawa H, Yanagida M, Wada O, Ogawa S, Nakagomi M, Oishi H, Yamamoto Y, Nagasawa H, McMahon SB, Cole MD, Tora L, Takahashi N, Kato S (2002) Nuclear receptor function requires a TFTC-type histone acetyl transferase complex. *Mol Cell* **9:** 553–562

Yoshizawa T, Handa Y, Uematsu Y, Takeda S, Sekine K, Yoshihara Y, Kawakami T, Arioka K, Sato H, Uchiyama Y, Masushige S, Fukamizu A, Matsumoto T, Kato S (1997) Mice lacking the vitamin D receptor exhibit impaired bone formation, uterine hypoplasia and growth retardation after weaning. *Nat Genet* **16:** 391–396

THE JOURNAL OF BIOLOGICAL CHEMISTRY
Vol. 280, No. 4, Issue of January 28, pp. 2543–2549, 2005
Printed in U.S.A.

Circulating FGF-23 Is Regulated by 1α,25-Dihydroxyvitamin D_3 and Phosphorus *in Vivo**

Received for publication, August 4, 2004, and in revised form, September 27, 2004
Published, JBC Papers in Press, November 5, 2004, DOI 10.1074/jbc.M408903200

Hitoshi Saito‡§, Akira Maeda‡, Shu-ichi Ohtomo‡, Michinori Hirata‡, Kenichiro Kusano‡, Shigeaki Kato¶, Etsuro Ogata‖, Hiroko Segawa, Ken-ichi Miyamoto**, and Naoshi Fukushima‡**

*From the ‡Pharmaceutical Research Department II, Chugai Pharmaceutical Co., Ltd., Gotemba, Shizuoka 412-8513, Japan, the ¶Institute of Molecular and Cellular Biosciences, Tokyo University, 1-1-1 Yayoi, Bunkyo-ku, Tokyo 113-0032, Japan, the ‖Cancer Institute Hospital, 1-37-1 Kami-ikebukuro, Toshima-ku, Tokyo 170-8455, Japan, and the **Department of Molecular Nutrition, Institute of Health Bioscience, University of Tokushima Graduate School, 3-18-15 Kuramoto-cho, Tokushima 770-8503, Japan*

Fibroblast growth factor-23 (FGF-23), a novel phosphate-regulating factor, was elevated in hypophosphatemic patients with X-linked hypophosphatemic rickets/osteomalacia and also in patients with chronic kidney disease. These observations suggested the pathophysiological importance of FGF-23 on phosphate homeostasis. However, regulation of FGF-23 production is still unclear. We investigated effects of both dietary phosphorus and 1α,25-dihydroxyvitamin D_3 (1α,25$(OH)_2D_3$) on circulating FGF-23 *in vivo*. Administration of 1α,25$(OH)_2D_3$ dose-dependently increased serum FGF-23 in thyroparathyroidectomized rats without correlating with serum inorganic phosphorus or serum parathyroid hormone. On the other hand, vitamin D receptor null mice had very low serum FGF-23 and did not respond to the 1α,25$(OH)_2D_3$ administration. These observations suggested 1α,25$(OH)_2D_3$ directly or indirectly regulates circulating FGF-23. Serum FGF-23 had a strong correlation with serum inorganic phosphorus controlled by dietary phosphorus in 5/6 nephrectomized rats. High phosphate diet elicited a 5-fold increase in serum FGF-23 compared with sham-operated rats, whereas serum FGF-23 did not correlate with serum calcium or serum creatinine in 5/6 nephrectomized rats. Administration of 1α,25-dihydroxyvitamin D_3 also elicited a severalfold increase in serum FGF-23 in the uremic rats. Taken together, this shows that both serum phosphorus and 1α,25$(OH)_2D_3$ regulate circulating FGF-23 independent of each other. Therefore, we proposed there was a feedback loop existing among serum phosphorus, 1α,25$(OH)_2D_3$, and FGF-23, in which the novel phosphate-regulating bone-kidney axis integrated with the parathyroid hormone-vitamin D_3 axis in regulating phosphate homeostasis.

The parathyroid hormone-vitamin D_3 endocrine system, as well as dietary phosphorus, plays an important role in regulating renal and gastrointestinal absorption of phosphate. Recently, emerging evidence suggests that other systemic and/or paracrine/autocrine factors are present in bones for maintaining phosphate homeostasis, such as fibroblast growth factor-23 (FGF-23),[1] frizzled-related protein-4 (FRP-4), and matrix extracellular phosphoglycoprotein (MEPE) (1–11). These three factors were highly expressed in tumors isolated from oncogenic osteomalacia patients and reduced phosphate transport in kidney. Among these factors, FGF-23 strongly suppressed 1α,25$(OH)_2D_3$ production and elicited hypophosphatemia. Administration of the recombinant FGF-23 protein reduced serum phosphorus without affecting serum calcium, as well as increasing renal phosphorus excretion in mice (12). Mice bearing FGF-23-expressing Chinese hamster ovary cells showed suppressed 25-hydroxyvitamin D_3 1α-hydroxylase mRNA expression in the kidney (3). FGF-23 mRNA is expressed in a variety of tissues such as thymus, brain, bone, thyroid/parathyroid gland, and heart (2, 3, 13). Recent studies (13, 14) indicated FGF-23 mRNA as well as FGF-23 protein was elevated in bones from patients with McCune-Albright syndrome and also in bones from HYP mouse, mouse homologue to X-linked hypophosphatemic (XLH) rickets. However, the level of serum FGF-23 in hypophosphatemic patients with XLH is still controversial (15–17). Hyperphosphatemic patients with chronic kidney disease showed significant elevation in circulating FGF-23, which correlated with serum phosphorus and creatinine (16, 18–20), suggesting (*a*) serum phosphorus was a possible regulator of FGF-23 production or (*b*) circulating FGF-23 accumulated in chronic renal failure.

The purpose of this study was to evaluate the effects of dietary phosphorus and 1α,25$(OH)_2D_3$ on FGF-23 production. Administration of FGF-23 protein or overexpression of *Fgf23* gene in rodent suppressed 1α,25$(OH)_2D_3$ production by reducing 25-hydroxyvitamin D_3 1α-hydroxylase in the proximal tubules (12, 21–23). On the contrary, *Fgf23*-null mice reported increased circulating 1α,25$(OH)_2D_3$ despite hyperphosphatemia, hypercalcemia, and low PTH levels (24). Administration of 1α,25$(OH)_2D_3$ increased serum FGF-23 in normal mice (25). These observations suggested mutual regulation between FGF-23 and 1α,25$(OH)_2D_3$; however, 1α,25$(OH)_2D_3$ administration also increases intestinal phosphate uptake and suppresses PTH. Thus, we used thyroparathyroidectomized rats as well as 5/6 nephrectomized rats fed a diet with various kinds of phosphorus content to examine the direct effect of 1α,25$(OH)_2D_3$ administration on serum FGF-23.

* The costs of publication of this article were defrayed in part by the payment of page charges. This article must therefore be hereby marked "*advertisement*" in accordance with 18 U.S.C. Section 1734 solely to indicate this fact.

§ To whom correspondence should be addressed. Tel.: 81-550-87-6735; Fax: 81-550-87-5326; E-mail: saitohts@chugai-pharm.co.jp.

[1] The abbreviations used are: FGF-23, fibroblast growth factor-23; P_i, phosphate; IP, inorganic phosphorus; TPTX, thyroparathyroidectomy; XLH, X-linked hypophosphatemia; *PHEX*, phosphate-regulating gene with homologies to endopeptidases on the X chromosome; 1α,25$(OH)_2D_3$, 1α,25-dihydroxyvitamin D_3; 1α-OHase, 25-hydroxyvitamin D_3 1α-hydroxylase; PTH, parathyroid hormone; ELISA, enzyme-linked immunosorbent assay; VDRKO, vitamin D receptor null(−/−).

Dietary phosphate deprivation or loading rapidly induces activation or repression of phosphate absorption in kidney and in intestine, mainly by inducing or suppressing type II sodium-dependent phosphate (Na/P_i) cotransporter expression (26, 27). Therefore, the serum phosphorus level is not susceptible to the change in dietary phosphorus content in normal animals *in vivo*. We investigated the effects of dietary phosphorus on FGF-23 production *in vivo* using 5/6 nephrectomized uremic rats, in which the serum phosphorus level can be easily manipulated by dietary phosphorus due to reduced kidney function. We also examined the correlations between serum FGF-23 and (*a*) serum inorganic phosphorus, (*b*) serum calcium, (*c*) serum creatinine, and (*d*) serum PTH in 5/6 nephrectomized rats.

EXPERIMENTAL PROCEDURES

Normal Rat—Eight-week-old male Sprague-Dawley rats (CREA Japan, Inc., Shizuoka, Japan) were given either vehicle, 10, 30, 100, or 300 ng of $1\alpha,25(OH)_2D_3$/kg of bodyweight intravenously, three times a week for 2 weeks. Blood samples were obtained from the vena cava under ether anesthesia on day 14. Serum calcium, serum inorganic phosphorus, and serum creatinine were measured by an automatic analyzer (Type 7170E, Hitachi Corp.). Serum FGF-23 was determined by the Human FGF-23 ELISA kit (Kinos Inc., Tokyo, Japan).

Thyroparathyroidectomized (TPTX) Rats and PTH-infused TPTX Rats—Eight-week-old male Sprague-Dawley rats purchased from Charles River (Tokyo, Japan) were TPTX under ether anesthesia. After confirming hypocalcemia had been induced, rats were divided to two groups, the TPTX group and the TPTX + PTH group. Rats in the TPTX + PTH group were subcutaneously implanted with ALZET® osmotic pumps (model 2ML2, Durect Corp., Cupertino, CA) and administered human PTH-(1–34) at a constant rate of 2.4 μg/day for 14 days. Rats in the TPTX group were intravenously injected with vehicle, 50 ng/kg or 300 ng/kg $1\alpha,25(OH)_2D_3$, three times a week for 2 weeks; rats in the TPTX + PTH group were injected with either vehicle or 50 ng/kg $1\alpha,25(OH)_2D_3$ three times a week for 2 weeks. Blood samples were collected and various parameters analyzed as described above.

Vitamin D Receptor Null(−/−) (VDRKO) Mice—VDRKO mice and their littermates kept on a high calcium and high phosphorus diet (28) were administered vehicle or 300 ng/kg $1\alpha,25(OH)_2D_3$ three times a week for 2 weeks. Blood samples were collected and analyzed as described above.

5/6 Subtotally Nephrectomized Uremic Rat Models and Diets—Male Sprague-Dawley rats weighing 180–200 g were purchased from CREA Japan and maintained under specific pathogen-free conditions with a 12-h light/dark cycle. After acclimating for 1 week, the rats were 5/6 nephrectomized and then allowed unlimited access to normal rodent chow (CE-2, CREA Japan Inc.) and tap water. The phosphate (P_i)-controlled diets and $1\alpha,25(OH)_2D_3$ injection started when rat serum creatinine reached within the range of 1.1–1.5 mg/dl. Three P_i-controlled diets (Oriental Yeast Co., Ltd., Osaka, Japan) were used in the present study: a high P_i diet, containing 0.9% phosphorus, 0.6% calcium; a midrange P_i diet, containing 0.6% phosphorus, 0.6% calcium; and a low P_i diet, containing 0.2% phosphorus, 0.6% calcium (26, 27).

The following groups of rats were studied: 1) 5/6 nephrectomized rats fed either the high, midrange, or low P_i diet for 4 weeks, 2) 5/6 nephrectomized rats fed the high, midrange, or low P_i diet and injected with 50 ng of $1\alpha,25(OH)_2D_3$/kg of bodyweight intravenously twice weekly for 4 weeks, and 3) age-matched sham-operated rats fed normal rat chow (CE-2, CREA Japan) used as a control. Blood samples were obtained from the vena cava under ether anesthesia at day 28 and various parameters analyzed as described above. Serum PTH was determined using a Rat Intact PTH ELISA kit (Immutopics, Inc., San Clemente, CA).

All animal procedures were conducted in accordance with Chugai Pharmaceutical's ethical guidelines for animal care, and all experimental protocols were approved by the Animal Care Committee of the institution.

Statistical Analysis—Data were expressed as means ± S.E., and statistical significance was determined using Student's *t* test or Dunnett's *t* test (SAS Preclinical Package, Version 5.0, SAS Institute Japan, Tokyo) unless otherwise indicated. A *p* value of <0.05 was considered statistically significant.

RESULTS

Effect of $1\alpha,25(OH)_2D_3$ on Serum FGF-23 in Normal Rats—Intravenous administration of $1\alpha,25(OH)_2D_3$, three times a week for 2 weeks, dose-dependently increased serum FGF-23 (Fig. 1*A*); however, it also increased serum inorganic phosphorus (Fig. 1*B*). Therefore, $1\alpha,25(OH)_2D_3$ administration increased both serum FGF-23 and serum phosphorus in normal rats.

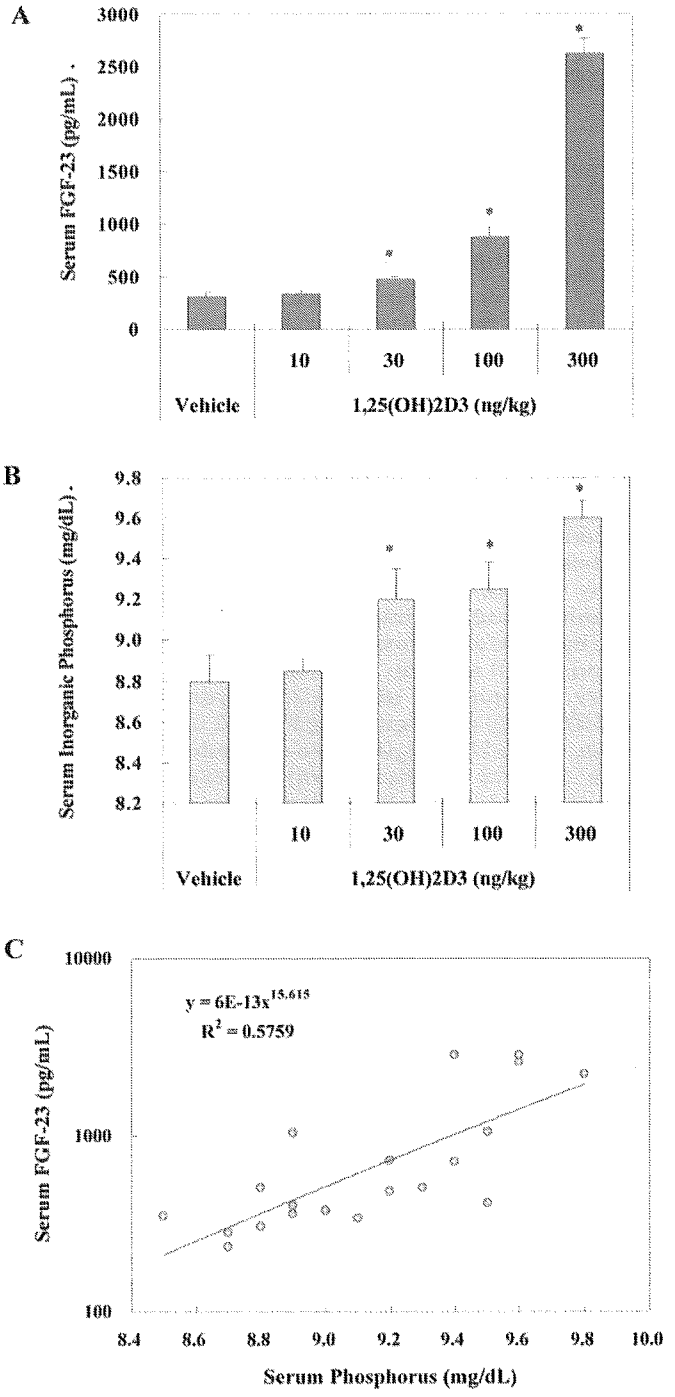

FIG. 1. Administration of $1\alpha,25$-dihydroxyvitamin D_3 dose-dependently increased both (*A*) serum FGF-23 as well as (*B*) serum inorganic phosphorus in normal rats. Correlation between serum FGF-23 and serum inorganic phosphorus in normal rats (*C*). Eight-week-old rats were given intravenously either vehicle, 10, 30, 100, or 300 ng/kg $1\alpha,25$-dihydroxyvitamin D_3 three times a week for 2 weeks. Serum inorganic phosphorus and FGF-23 were determined as described in the text. Each column represents mean ± S.E. ($n = 4$). *, statistically significant *versus* vehicle; $p < 0.05$, by Dunnett's *t* test.

Effects of $1\alpha,25(OH)_2D_3$ on Serum FGF-23 in TPTX Rats—As shown in Fig. 2, *A–C*, Thyroparathyroidectomized rats induced hyperphosphatemia, hypocalcemia, and also a slight but signif-

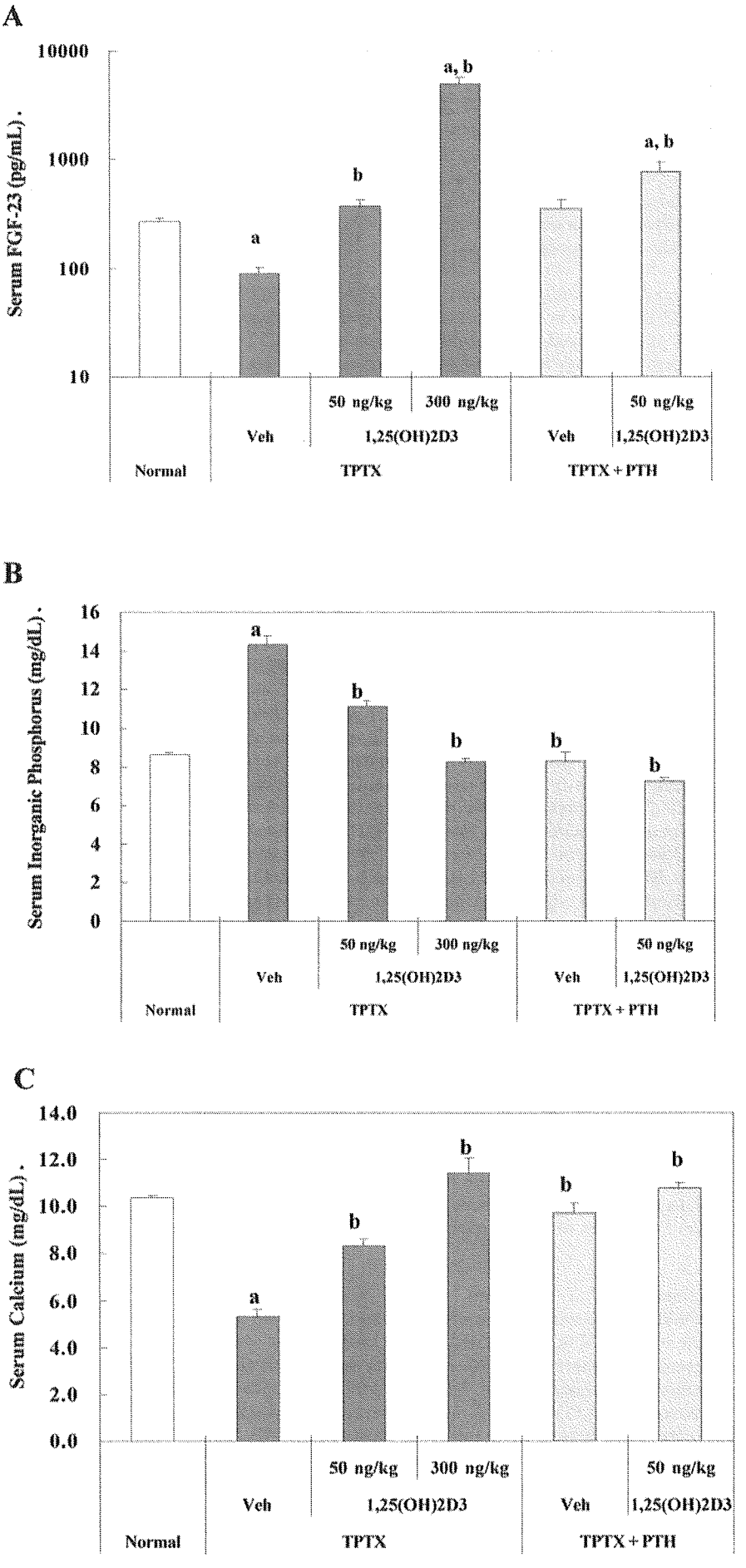

FIG. 2. **Effect of 1α,25-dihydroxyvitamin D_3 on serum FGF-23 (*A*), serum inorganic phosphorus (*B*), and serum calcium (*C*) in TPTX rats.** TPTX or PTH-infused TPTX rats were given intravenously vehicle (*Veh*) or 1α,25-dihydroxyvitamin D_3 three times a week for 2 weeks. Serum inorganic phosphorus, calcium, and FGF-23 were determined as described under "Experimental Procedures." Each column represents mean ± S.E. (n = 4–5). *a*, statistically significant *versus* normal; *b*, *versus* TPTX vehicle treatment; $p < 0.05$, by Student's t test.

icant decrease in serum FGF-23 in comparison with normal rats. Administration of $1\alpha,25(OH)_2D_3$ dose-dependently increased serum FGF-23 as well as serum calcium in TPTX rats. Also $1\alpha,25(OH)_2D_3$ suppressed serum inorganic phosphorus in TPTX rats. PTH infusion to TPTX rats normalized serum calcium, serum inorganic phosphorus, and serum FGF-23. $1\alpha,25(OH)_2D_3$ increased serum FGF-23; however, unlike TPTX rats, no significant change was observed in serum inorganic phosphorus and serum calcium in PTH-infused TPTX rats. These observations suggested that $1\alpha,25(OH)_2D_3$ increased serum FGF-23 independent of serum inorganic phosphorus and PTH.

Effect of $1\alpha,25(OH)_2D_3$ on Serum FGF-23 in VDRKO Mice—VDRKO mice kept on high calcium (2%) and high phosphorus (1.25%) diets showed considerably low serum FGF-23 (<3 pg/ml, below detection limit) and low serum calcium (5.8 ± 0.6 mg/dl) in comparison with the wild-type littermates (FGF-23, 254 ± 35.6 pg/ml; calcium, 9.5 ± 0.1 mg/dl). $1\alpha,25(OH)_2D_3$ administration did not affect either serum FGF-23 (<3 pg/ml, below detection limit) or serum calcium (5.1 ± 0.2 mg/dl).

Effects of P_i-controlled Diets on Serum FGF-23 and Serum Inorganic Phosphorus in 5/6 Nephrectomized Rats—Serum inorganic phosphorus correlated with the dietary phosphorus contents (Fig. 3*A*) in 5/6 nephrectomized rats. On the contrary, serum calcium correlated with serum phosphorus in a reciprocal fashion (Fig. 3*B*). The 5/6 nephrectomy induced a significant increase in serum FGF-23 in rats, regardless of the dietary phosphorus contents (Fig. 3*C*). Serum FGF-23 of sham-operated rats was 305 ± 23 pg/ml. Whereas, serum FGF-23 increased in high, midrange, and low P_i diet groups (5108 ± 989 pg/ml, 1815 ± 200 pg/ml, and 1133 ± 121 pg/ml, respectively). Serum FGF-23 showed a clear correlation with serum phosphorus (Fig. 4*A*) and a weak inverse correlation with serum calcium (Fig. 4*B*) in 5/6 nephrectomized rats. However, serum FGF-23 did not correlate with serum creatinine (Fig. 4*C*).

Effect of $1\alpha,25(OH)_2D_3$ on Serum FGF-23 and Serum Inorganic Phosphorus in 5/6 Nephrectomized Rats—Serum FGF-23 in the 5/6 nephrectomized rats on each P_i-controlled diet was augmented significantly by the administration of $1\alpha,25(OH)_2D_3$ (Fig. 5). $1\alpha,25(OH)_2D_3$ administration also increased serum inorganic phosphorus, serum calcium, and serum creatinine and decreased serum PTH in all diet groups (data not shown). Serum inorganic phosphorus weakly correlated with serum FGF-23 in the nephrectomized rats with or without $1\alpha,25(OH)_2D_3$ treatment (Fig. 6*A*). However, the other three parameters did not have a strong correlation with serum FGF-23 (Fig. 6, *B–D*).

In normal rats, 30 and 100 ng/kg $1\alpha,25(OH)_2D_3$ injection increased serum FGF-23 only by 1.5- and 3-fold, respectively. Whereas, in the 5/6 nephrectomized rats, 50 ng/kg $1\alpha,25(OH)_2D_3$ increased serum FGF-23 by 3–9-fold, suggesting that $1\alpha,25(OH)_2D_3$ had a more profound effect on increasing serum FGF-23 in rats with chronic renal failure.

DISCUSSION

Shimada *et al.* reported that a single injection of $1\alpha,25(OH)_2D_3$ increased serum FGF-23 and suggested the increase in FGF-23 by $1\alpha,25(OH)_2D_3$ was independent of serum inorganic phosphorus (25). We confirmed their result that intravenous administration of $1\alpha,25(OH)_2D_3$ dose-dependently increased serum FGF-23 (Fig. 1*A*). However, we also observed an increase in serum inorganic phosphorus (Fig. 1*B*). There was a strong significant correlation between serum FGF-23 and serum phosphorus (Fig. 1*C*) in the normal rats given $1\alpha,25(OH)_2D_3$. Since $1\alpha,25(OH)_2D_3$ stimulates intestinal phosphate uptake and suppresses PTH production, this experiment indicated that $1\alpha,25(OH)_2D_3$ increased serum FGF-23 as well

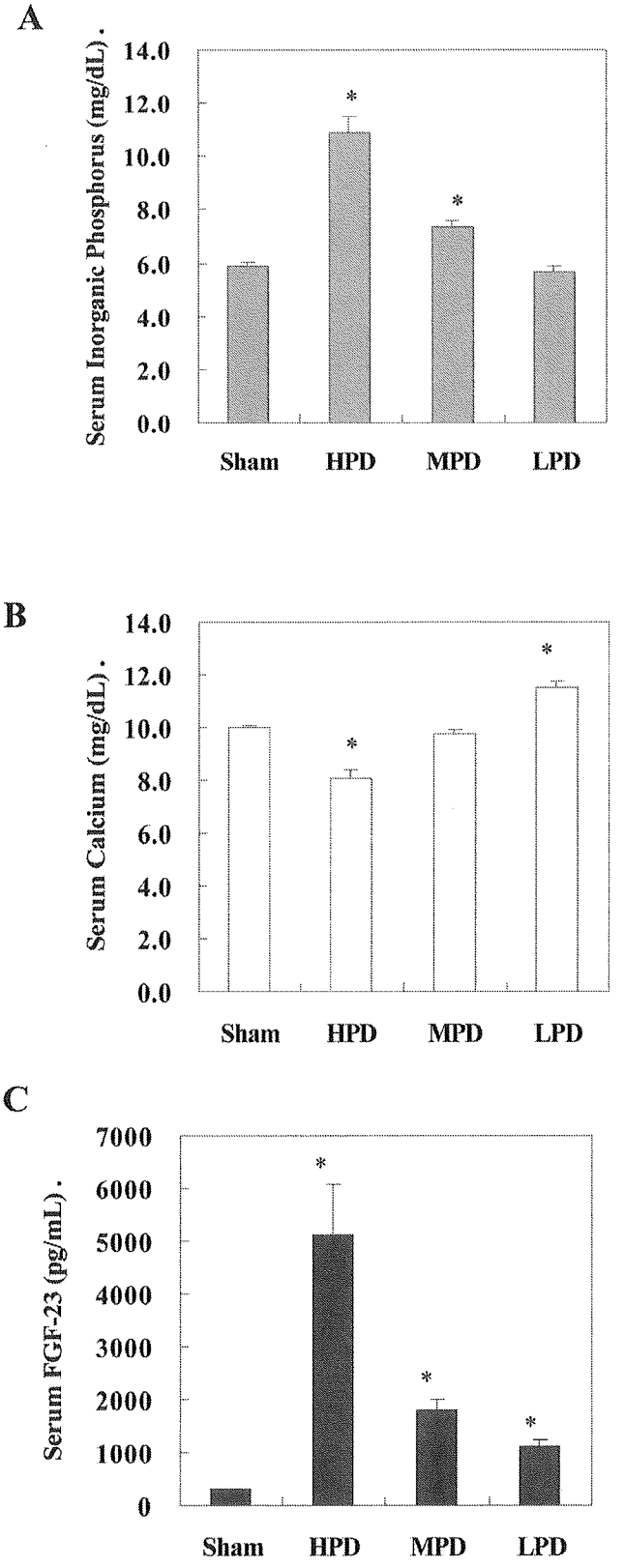

FIG. 3. **Effect of P_i-controlled diet on serum inorganic phosphorus, serum calcium, and serum FGF-23 in 5/6 nephrectomized rats.** 5/6 nephrectomized rats were fed either high P_i (0.9% P_i, 0.6% calcium) diet (*HPD*), midrange P_i (0.6% P_i, 0.6% calcium) diet (*MPD*), or low P_i (0.2% P_i, 0.6% calcium) diet (*LPD*) for 4 weeks. Blood samples were taken on day 28 from the vena cava under ether anesthesia. Serum inorganic phosphorus, serum calcium, and serum FGF-23 were determined as described under "Experimental Procedures." Data represents means ± S.E. (sham-operated group, $n = 5$; 5/6 nephrectomized groups, $n = 10$). *, statistically significant in comparison with the sham-operated group, $p < 0.05$ by Student's t test.